Imaging Momentum Orbital Densities of Conformationally Versatile Molecules: A Benchmark Theoretical Study of the Molecular and Electronic Structures of Dimethoxymethane

Y. R. Huang,[†,‡] S. Knippenberg,[†] B. Hajgató,[†] J.-P. François,[†] J. K. Deng,[‡] and M. S. Deleuze*,[†]

Research group of Theoretical Chemistry, Department SBG, University of Hasselt, Agoralaan, Gebouw D, B3590 Diepenbeek, Belgium, and Department of Physics and Key Laboratory of Atomic and Molecular NanoSciences of MOE, Tsinghua University, Beijing 100084, P. R. China

Received: March 12, 2007; In Final Form: April 11, 2007

The main purpose of the present work is to predict from benchmark many-body quantum mechanical calculations the results of experimental studies of the valence electronic structure of dimethoxymethane employing electron momentum spectroscopy, and to establish once and for all the guidelines that should systematically be followed in order to reliably interpret the results of such experiments on conformationally versatile molecules. In a first step, accurate calculations of the energy differences between stationary points on the potential energy surface of this molecule are performed using Hartree−Fock (HF) theory and post-HF treatments of improving quality (MP2, MP3, CCSD, CCSD(T), along with basis sets of increasing size. This study focuses on the four conformers of this molecule, namely the trans−trans (TT), trans−gauche (TG), gauche−gauche (G^+G^+), and gauche−gauche (G^+G^-) structures, belonging to the C_{2v}, C_1, C_2, and C_s symmetry point groups, respectively. A focal point analysis supplemented by suited extrapolations to the limit of asymptotically complete basis sets is carried out to determine how the conformational energy differences at 0 K approach the full CI limit. In a second step, statistical thermodynamics accounting for hindered rotations is used to calculate Gibbs free energy corrections to the above energy differences, and to evaluate the abundance of each conformer in the gas phase. It is found that, at room temperature, the G^+G^+ species accounts for 96% of the conformational mixture characterizing dimethoxymethane. In a third step, the valence one-electron and shake-up ionization spectrum of dimethoxymethane is analyzed according to calculations on the G^+G^+ conformer alone by means of one-particle Green's function [1p-GF] theory along with the benchmark third-order algebraic diagrammatic construction [ADC(3)] scheme. A complete breakdown of the orbital picture of ionization is noted at electron binding energies above 22 eV. A comparison with available (e,2e) ionization spectra enables us to identify specific fingerprints of through-space orbital interactions associated with the anomeric effect. At last, based on our 1p-GF/ADC(3) assignment of spectral bands, accurate and spherically averaged (e,2e) electron momentum distributions at an electron impact energy of 1200 eV are computed from the related Dyson orbitals. Very significant discrepancies are observed with momentum distributions obtained for several outer-valence levels using standard Kohn−Sham orbitals.

Introduction

Electron momentum spectroscopy (EMS)[1] has been extensively used for studying the valence electronic structures and wave functions of small polyatomic molecules with typically one, two, or three "heavy" (C, N, O, ...) atoms,[2] or larger but structurally rigid molecules of high and well-defined symmetry,[3] such as benzene, sulfur hexafluoride, transition metal carbonyls ($X(CO)_6$ with X = Cr, Mo, or W), fullerene, furan, pyrrole, norbornadiene, cubane, chlorotrifluoromethane, adamantane, amantadine, isobutane, urotropine, pyridine, or norbornane. With this very sophisticated spectroscopic technique based on electron impact ionization experiments at high kinetic energies, one can reliably infer electron momentum distributions associated with (in principle, carefully) selected ionization channels, from an analysis of the angular dependence of (e,2e) ionization intensities measured in coincidence at fixed electron binding energies. Because of the still limited energy resolution of the spectrometers (at best, ∼0.6 eV) and of the difficulties inherent in assigning overcrowded ionization bands, interpretations of EMS experiments on large systems remain very challenging. In addition, the energies required by valence ionization processes are considerable, and most often are larger than those involved in, for instance, chemical reactions (typically, a few electronvolts). We note that many of the above listed compounds are cage compounds subject to pronounced cyclic strains, which may lead to severe vibrational complications and, in the most extreme cases, to ultrafast intramolecular rearrangements and Coulomb explosion processes at electron binding energies above the double ionization threshold.[3p]

Sophisticated quantum mechanical treatments that cope, at least, with electron correlation and relaxation effects, as well as with the dispersion of the ionization intensity over shake-up states arising from configuration interaction effects in the cation,[4] are therefore the most basic requirement for reliably assigning (e,2e) ionization spectra and conducting from these a safe analysis of experimental electron momentum distributions. A

* To whom correspondence should be addressed. E-mail: michael.deleuze@uhasselt.be.
† University of Hasselt.
‡ Tsinghua University.

10.1021/jp0719964 CCC: $37.00
Published on Web 06/13/2007

recent revision by our group of EMS measurements on a series of cage compounds demonstrates that it is indeed impossible to reliably assign highly congested (e,2e) ionization spectra by resorting only to standard Hartree−Fock or Kohn−Sham orbital energies and to the related electron densities.[5] Furthermore, most molecules of interest in chemistry exist in more than one stable conformation, which complicates further the analysis of the (e,-2e) ionization spectra and intensities.[6,7] The reader is referred in particular to a pioneering and very detailed analysis[8] by our group of EMS experiments[9,10] upon a highly versatile molecule, namely, *n*-butane, employing statistical thermodynamics[11] at the level of the rigid rotor−harmonic oscillator (RRHO) approximation as well as one-electron Green's function theory[12−16] (also referred to as electron propagator theory) along with the so-called third-order algebraic diagrammatic construction scheme [ADC(3)].[15,17]

When dealing with molecules containing one or several rotatable bonds, such as biomolecules, it is crucial to correctly assess the relative abundance of conformers and the influence of the molecular conformation upon the valence ionization spectrum. Otherwise, when failing to correctly assign the ionization bands and their relationships with one or several conformers, one may draw conclusions that lead, for instance, to obvious violations of elementary principles of thermodynamics and contradictions with an impressive amount of spectroscopic evidence. A striking example has been recently discussed in detail through a robust refutation[18] of an analysis by Saha et al.[19] of EMS experiments on 1,3-butadiene.[20] The main purpose of the present work is to establish once and for all the guidelines that should be systematically followed for reliably interpreting the results of such measurements on conformationally versatile molecules. Note that it is cumbersome to *interpret* a posteriori EMS experiments from theoretical calculations. For the sake of credibility, we wish therefore to first *predict* in detail the electron momentum distributions that should be experimentally amenable from EMS measurements upon dimethoxymethane, throughout the valence region of this compound.

Dimethoxymethane, the prototype of polyethers, represents one of the cornerstones of molecular mechanics and conformational analysis.[21] This compound has been extensively studied as a model of the acetal moiety in methyl pyranosides and of the glycosidic linkage in polysaccharides. Its potential energy surface is usually described[22,23] in terms of four energy minima relating to the all-staggered (anti−anti or trans−trans, TT), trans−gauche (TG), gauche−gauche (G^+G^+) and gauche−gauche (G^+G^-) conformers (also referred to as rotamers; see Figure 1). The conformational behavior of dimethoxymethane is governed by dipole−dipole interactions and by the anomeric effect.[22−29] In a localized orbital picture, the latter is described as a through-space $n \rightarrow \sigma^*$ stabilizing frontier orbital interaction which tends to favor a coplanar alignment of one of the p-type electron lone pairs on oxygen atoms with the σ^* orbital of a vicinal C−O bond.

Electrostatic and hyperconjugation interactions explain the overall gauche preference of substituents about C−O bonds in sugars.[30,31] Unsurprisingly, therefore, the G^+G^+ rotamer is known to be the global energy minimum form of dimethoxymethane, according to a number of experiments employing dipole moment measurements,[32] electron diffraction,[33] nuclear magnetic resonance,[34] X-ray diffraction,[35] infrared spectroscopy in argon matrices,[23] or rotational spectroscopy.[36] Because of the anomeric effect, and of the usually very strong interplay between the molecular and electronic structures, dimethoxymethane could be a very ideal molecule for evaluating the so far largely

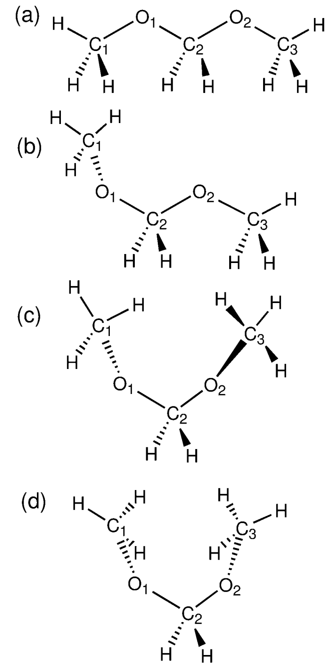

Figure 1. Geometries of the (a) TT (C_{2v} symmetry), (b) TG (C_1), (c) G^+G^+ (C_2), and (d) G^+G^- (C_s) conformers of dimethoxymethane.

unexploited potential of electron momentum spectroscopy (EMS) in experimentally "imaging" the distortions and topological changes that molecular orbitals undergo under internal rotations and variations of the molecular conformations, despite the correlation of electronic motions in many-electron systems and the fact that, even for systems containing only one electron, orbitals derived as eigenfunctions of one-electron Hamiltonians do not represent true molecular observables, as very pertinently noted by Prof. Schwarz.[37]

So far, experimental data about the electronic structure of dimethoxymethane are very scarce. These comprise the (He I) ultraviolet photoelectron spectrum by Jørgensen et al.[38] and the (e,2e) ionization spectrum that Neville et al. recorded about 10 years ago[6] at an electron impact of 1.2 keV. Note that the latter authors restricted their analysis of the related electron momentum distributions to the two outermost orbitals, presumably because accurate enough computations of the ionization spectra, relative energies, and thermodynamic state functions (enthalpy, entropy, etc.) characterizing fairly large molecular structures with limited symmetry, or even no symmetry at all, were not achievable or even conceivable at this time. In contrast with pioneering Hartree−Fock calculations in conjunction with the standard 4-31G basis set,[39] early theoretical investigations based on extended Hückel or semiempirical INDO or MINDO/2 calculations[40] failed to predict the correct energy minimum of dimethoxymethane, due to the inability of these schemes to describe hyperconjugation effects. The anomeric-driven G^+G^+ geometry has been thereafter confirmed at various ab initio levels.[41,42]

The most thorough quantum chemical studies available to date of the structures and relative energies of the various rotamers of dimethoxymethane were based on second-order Møller−Plesset calculations in conjunction with the 6-31G** basis set,[22] or calculations[22,23] employing density functional theory (DFT) along with the Becke three-parameter Lee−Yang−Parr (B3LYP) functional[43] and the 6-311++G** basis set. The obtained geometries are almost the same, but rather significant differences in relative energies, comprised within a range of a few kilocalories per mole, justify a more quantitative study of the main stationary points on the potential energy surface of dimethoxymethane. Extremely accurate energy differences are indeed obviously needed for reliably evaluating, within an accuracy of a few percent, the abundances of rotamers characterized by energies that do not differ by more than ~3 kcal/mol. Relative conformer energies are thus first evaluated within the confines of nonrelativistic quantum mechanics, by means of a focal point analysis[44−47] of results obtained using ab initio (Hartree−Fock,[48] Møller−Plesset,[48,49] coupled cluster[50]) methods and basis sets of improving quality. At the next step, conformer abundances at room temperature are evaluated for the gas phase from these benchmark energy differences, from zero-point harmonic vibrational corrections, and from accurate Gibbs free energy corrections derived from statistical thermodynamic partition functions[11] accounting for internal hindered rotations.[51] According to these calculations, it will be found that, at room temperature, the G^+G^+ species accounts for 96% of the conformational mixture characterizing dimethoxymethane, and that the contributions from the other conformers to the measured ionization intensities are thus negligible. Therefore, in a third step, the valence one-electron and shake-up ionization spectrum of the G^+G^+ conformer alone is calculated using one-particle Green's function [1p-GF] theory[13−16] along with the benchmark third-order algebraic diagrammatic construction [ADC(3)] scheme.[15,17] Experimentally resolvable (e,2e) ionization bands are correspondingly identified, taking into account line broadening as well as the influence of the azimuthal angle under which the emitted electrons are collected in coincidence upon the (e,2e) intensities. At last, based on our 1p-GF/ADC(3) assignment of the ionization spectrum, accurate and spherically averaged (e,2e) electron momentum distributions at an electron impact energy of 1200 eV are computed for each resolvable band from Dyson orbitals[52] that also readily derive from the 1p-GF/ADC(3) computations. For the sake of completeness, and to emphasize possible shortcomings of many recent theoretical analyses of EMS experiments, comparison is made with spherically averaged (e,2e) electron momentum distributions associated with Kohn−Sham orbitals deriving from DFT calculations employing the standard B3LYP functional.

Theory and Methodology

(a) Focal Point Analysis of Energy Differences. To quantitatively evaluate the relative energies and abundances, within the confines of nonrelativistic quantum mechanics, of the four known conformers of dimethoxymethane, we first analyze in detail the convergence of these energy differences upon successive and systematic improvements of the basis set and of the employed computational level. In straightforward analogy with former focal point analyses of conformational energy differences,[44,45] rotational barriers,[46] or ionization energies,[47] the faster convergence of the higher-order correlation corrections to the calculated energy differences is exploited in well-suited extrapolations of results obtained using CCSD(T) theory[50] (coupled cluster anzats including single and double electronic excitations and supplemented by a perturbative treatment of triple excitations). To be more specific, reliable estimations of CCSD(T) energy differences in the limit of an infinitely large basis set can be made by adding almost converged high-level correlation corrections, obtained at the MP3,[39] CCSD, and CCSD(T) levels with rather limited basis sets, to lower-level HF and MP2[38] results which are calculated in conjunction with the largest basis sets, along with suited extrapolation procedures. The employed basis sets comprise the standard Pople's basis sets, namely STO-3G, 6-31G, 6-31G*, 6-31G**, and 6-311G**, Dunning's correlation consistent polarized valence basis sets of double-, triple-, and quadruple-ζ quality, designated as cc-pVXZ, with X = D, (T, [Q]), respectively,[53] as well as an augmented version of the latter basis sets including a set of s, p, (d [f]) and s, p, d, (f [g]) diffuse functions on hydrogens, and carbons or oxygens, respectively.[54a] With the largest employed basis set (aug-cc-pVQZ), 768 basis functions were included in the calculations performed on each rotamer of dimethoxymethane. Depending on the symmetry point group, the MP3 calculations performed with this basis set required runs of 72−148 h (CPU time) on a powerful ES47 workstation (20 GB core memory, 660 GB disk, and two dual processors of 1 GHz). Other prohibitive calculations that are presented in this work were carried out on all four species at the CCSD(T)/aug-cc-pVTZ level [414 basis functions]. On the same work station, these required runs of 19−77 h (CPU time).

Estimates of the conformer energy differences have also been calculated in the asymptotic limit of an infinitely large basis set. For this purpose, we rely on well-suited extrapolations of the HF total electronic energies obtained for the neutral molecules and their cations using Dunning's series of cc-pVXZ basis sets, and, as suggested by Feller,[54] an exponential fit of the form

$$E(l) = E_\infty + A\mathrm{e}^{-Bl} \qquad (1)$$

where the cardinal number l equals 2, 3, 4, ... when X = D, T, Q, ..., respectively. In turn, correlated total energies are extrapolated to an asymptotically complete basis set by means of a three-point extension (named Schwartz 6(lmn)[55]) of Schwartz's extrapolation formula,[56] which is based on inverse powers of (l + (1/2)):

$$E(l) = E_\infty + \frac{B}{\left(l + \frac{1}{2}\right)^4} + \frac{C}{\left(l + \frac{1}{2}\right)^6} \qquad (2)$$

All the calculated energy differences derive from single-point calculations performed upon geometries optimized using DFT, along with the B3LYP functional and the aug-cc-pVTZ basis set. At this stage, we would like to recall that, compared with experiment or benchmark theoretical results, the B3LYP predictions for bond lengths and bond angles are generally superior to the MP2 ones.[57] As such, B3LYP geometries are often retained in rigorous theoretical models aiming at chemical accuracy (see, e.g., ref 58 for a review of the design and applications of the so-called Weizmann-1 theory). Indeed, the B3LYP approach is known to provide structural as well as harmonic vibrational frequencies of quality comparable to the CCSD(T) level (see also ref 59).

(b) Calculation of Conformer Abundances. Based on our best estimates of the relative energies of the four conformers of dimethoxymethane, the relative abundances of each species are estimated according to Boltzmann statistical thermodynamics, using the standard formula

$$n_i = \rho_i \exp(-\Delta G_i/RT) \qquad (3)$$

with ρ_i the multiplicity (or symmetry number) of the species of interest on the potential energy surface of dimethoxymethane. Here, ΔG_i values denote our best estimates for the Gibbs free energy of the species of interest relative to the most stable conformer (G^+G^+). More specifically, these quantities have been obtained by adding to the benchmark quantum mechanical energy differences, obtained from the above-described focal point analysis, B3LYP/aug-cc-pVTZ zero-point vibrational energy corrections, as well as enthalpy and entropy corrections derived from Boltzmann statistical thermodynamics, using electronic, rotational, and vibrational partition functions that were also computed at the B3LYP/aug-cc-pVTZ level, at standard temperature (298 K) and pressure (1 atm). The evaluation reported here goes beyond the (uncoupled) rigid rotor–harmonic oscillator (RRHO) approximation, as hindered rotations are accounted for by means of the protocol by Ayala and Schlegel[60] for identifying and treating the internal rotation modes, using a projection of harmonic vibrational normal modes on constrained stretches, bends, and out-of-plane motions, leaving only the torsion modes, as well the rules of Mayo, Olafson, and Goddard[61] for obtaining the potential periodicity, the rotating tops' symmetry numbers, and the well multiplicities. The protocol by Ayala and Schlegel[60] also employs an improved analytical approximation, according to a best-fit procedure, of the formula of Pitzer and Gwinn[51a] for the partition function associated with one-dimensional hindered internal rotations.

All Hartree–Fock (HF), DFT, and thermodynamic calculations described so far have been performed using the Gaussian 03 package of programs.[62] The Møller–Plesset (MP) and coupled cluster (CC) single-point calculations were performed using the MOLPRO 2000.1 package of programs.[63]

(c) Ionization Spectra. At the 1p-GF/ADC(3) level, the calculation of one-electron and shake-up ionization energies implies solving a secular problem of the form $\mathbf{HX} = \mathbf{XE}$ (with $\mathbf{XX}^\dagger = 1$), in which the secular matrix $\mathbf{H}$ reads

$$\mathbf{H} = \begin{bmatrix} \epsilon + \mathbf{\Sigma}(\infty) & \mathbf{U}^+ & \mathbf{U}^- \\ (\mathbf{U}^+)^\dagger & \mathbf{K}^+ + \mathbf{C}^+ & \mathbf{0} \\ (\mathbf{U}^-)^\dagger & \mathbf{0} & \mathbf{K}^- + \mathbf{C}^- \end{bmatrix} \tag{4}$$

This matrix is cast over 1h and excited (shake-up) 2h-1p states (+) as well as over 1p and excited (shake-on) 2p-1h anionic states (−). To achieve a through-third-order treatment of one-electron ionization processes, the block matrices $\mathbf{K}^+ + \mathbf{C}^+$ ($\mathbf{K}^- + \mathbf{C}^-$) are derived through first-order in correlation as effective configuration interactions between the 2h-1p shake-up (2p-1h shake-on) states. The vectors of coupling amplitudes, $\mathbf{U}^+$ ($\mathbf{U}^-$) between the 2h-1p (2p-1h) and 1h (1p) states are derived through second-order in correlation. $\mathbf{\Sigma}(\infty)$ is the static self-energy describing the electrostatic potential felt by an outgoing or ingoing electron due to correlation corrections to the Hartree–Fock (HF) ground state one-electron density. This potential has been computed through fourth-order in correlation, using charge-consistent one-electron densities.[64]

The ADC(3) calculations have been carried out using the original 1p-GF/ADC(3) package of programs, interfaced to GAMESS.[65] This package incorporates a band-Lanczos[66] "pre"diagonalization of the block matrices pertaining to the 2p-1h shake-on states into a pseudo-electron attachment spectrum, prior to a complete block-Davidson diagonalization[67] of the so-reduced ADC(3) secular matrix. With this diagonalization procedure, all eigenvalues of the ADC(3) secular matrix with pole strengths equal to or greater than 0.005 could be recovered up to electron binding energies of ~30 eV. The assumption of frozen core electrons has been used throughout and the full molecular symmetry point groups have been exploited. At the self-consistent-field level, the requested convergence on each of the elements of the density matrix was fixed to 10^{-10}. The 1p-GF/ADC(3) calculations have been carried out using Dunning's correlation-consistent polarized valence basis set of double-ζ quality (cc-pVDZ).[53a] To assess the effect of diffuse functions on Dyson orbital momentum distributions, an attempt to use the aug-cc-pVDZ basis with diffuse functions centered on hydrogen, carbon, and oxygen atoms was also made. However, severe linear dependencies resulting in divergency problems prevented us from successfully completing ADC(3) calculations with the latter basis set, which led us to drop d-type diffuse functions on carbon and oxygen atoms in the original aug-cc-pVDZ basis set, giving rise to a slightly smaller diffuse basis set referred to as the cc-pVDZ++ one.

The ionization spectra presented in the sequel have been simulated using as convolution function a combination of a Gaussian and a Lorentzian with equal weight (Voigt profile) and a constant full width at half-maximum parameter (fwhm) of 0.6 or 1.1 eV. The latter parameters have been selected in order to enable comparisons with available experimental data obtained by means of ultraviolet (He I) photoelectron spectroscopy (UPS) or electron momentum spectroscopy, respectively, taking into account the energy resolutions that can be achieved for both spectroscopies nowadays, as well as natural and vibrational broadening.

(d) (e,2e) Ionization Intensities and Spherically Averaged Electron Momentum Distributions. Electron momentum spectroscopy[1] is based on electron impact ionization experiments focusing on (e,2e) reactions ($M + e^- \rightarrow M^+ + 2e^-$) at high kinetic energies ($E_0 \gg 1$ keV, with E_0 the energy of the impinging electron). Under the assumptions of the Born, binary encounter, and plane wave impulse approximations,[1] the (e,2e) ionization cross sections are directly proportional to structure factors derived as the Fourier transforms of Dyson orbitals for the ionization channels under consideration:

$$\sigma_n = K \int |g_n(\omega,p)|^2 \, d\Omega \tag{5}$$

where ω and p represent the spin and momentum of the electron *prior* to ionization. In the above equation, $\int d\Omega$ denotes the spherical average over all orientations of the target molecule. Using spin-space coordinates $\mathbf{x} = (\omega,\vec{r})$, Dyson spin–orbitals orbitals are defined[52] as partial overlaps between the initial neutral ground state and final ionized states:

$$g_n(\mathbf{x}) = \sqrt{N} \int \Psi_n^{N-1}(\mathbf{x}_1,\mathbf{x}_2,...,\mathbf{x}_{N-1}) \Psi_0^N(\mathbf{x}_1,\mathbf{x}_2,...,\mathbf{x}_{N-1},\mathbf{x}) \, d\mathbf{x}_1 \, d\mathbf{x}_2 \, ... \, d\mathbf{x}_{N-1} \tag{6}$$

with N the number of electrons. These spin–orbitals $g_n(\mathbf{x})$ can therefore be regarded as effective orbitals for the holes created in the cationic states $|\Psi_n^{N-1}\rangle$, which account both for ground state correlation and dynamic relaxation effects, as well as for the dispersion of the ionization intensity over states relating to excited (shake-up) electronic configurations of the cation: by definition, the norm of Dyson orbitals is smaller than 1. Note that eqs 5 and 6 provide a *formally exact depiction* of (e,2e) cross sections in the high-energy limit ($E_0 \gg 1$ keV), ensuring the so-called EMS conditions.[1] In practice, although the required energy is still under debate,[68] the employed value for E_0 ranges, in most applications, from 1.2 to 1.6 keV.

Assuming that the usual symmetric non-coplanar geometric setup[1c] is used for characterizing in coincidence the kinematics of (e,2e) ionization events, and that the binary encounter requirements of high impact energy, high momentum transfer, and negligible kinetic energy transfer to the residual ion are therefore fulfilled, the initial momentum p of the knocked-out electron can be monitored by scanning the azimuthal angle (ϕ) under which the electrons are selected, according to basic conservation laws on momenta and energies:

$$p = \sqrt{(2p_1 \cos\theta - p_0)^2 + (2p_1 \sin\theta \sin(\phi/2))^2} \qquad (7)$$

and

$$E_1 + E_2 = E_0 - E_n = E_{\mathrm{Total}} \qquad (8)$$

with E_1 (p_1) and E_2 (p_2) the energies (momenta) of the two outgoing electrons, and where $\theta = \theta_1 = \theta_2 = 45°$ define the polar angles used in the experiment. In these equations, according to the characteristics of the experimental setup employed at Tsinghua University,[69] the relevant parameters amount to $p_1 = p_2 = 6.64077$ au, $p_0 = 0.271105\,(1200 + E_n)^{1/2}$ au (1 au $= 1a_0^{-1}$ with a_0 the Bohr radius, i.e., 0.5292 Å), $E_{\mathrm{Total}} = 1200$ eV, and $E_1 = E_2 = 600$ eV. In this setup, the azimuthal angle ϕ varies from $-38°$ to $38°$, which enables measurements of (e,2e) ionization intensities up to electron momenta of $\sim$3.0 au. In the latter equation, E_n is the electron binding energy characterizing the ionization channel of interest (from here and henceforth, the label n defines the final ionized state). Therefore, measuring (e,2e) intensities over a *fixed* range of ionization energies as a function of the azimuthal angle enables us in practice to construct experimental electron momentum distributions related to the corresponding set of ionization channels. Note in particular that, for a zero electron binding energy ($E_n = 0$ eV), $\phi = 0°$ implies that $p = 0$ au.

In practice, Dyson orbitals can always be expanded as a linear combination of HF orbitals $|\phi_i\rangle$:

$$g_n(\mathbf{x}) = \frac{1}{\sqrt{\Gamma_n}} \langle \Psi_n^{N-1} | \Psi_0^N \rangle_{N-1} = \frac{1}{\sqrt{\Gamma_n}} \sum_i x_i^{(n)} \phi_i(\mathbf{x}) \qquad (9)$$

where the suffix $N - 1$ emphasizes[4e] partial integration over $N - 1$ electron spin-space coordinates ($\mathbf{x}$) (see eq 6). In the above equation, the weight coefficients $x_i^{(n)}$ relate to Feynman−Dyson transition amplitudes.

$$x_i^{(n)} = \langle \Psi_n^{N-1} | a_i | \Psi_0^N \rangle \qquad \forall\, n \in \{N - 1\} \qquad (10)$$

with a_i the operator describing the annihilation of an electron in orbital ϕ_i. Note that, in eq 9, spectroscopic (pole) strengths Γ_n defining the probability to observe a given ionic state $|\Psi_n^{N-1}\rangle$ have been used to normalize the Dyson orbitals, and enable therefore consistent comparisons with (by construction, normalized) Hartree−Fock or Kohn−Sham orbital momentum densities:

$$\Gamma_n = ||\langle \Psi_n^{N-1} | \Psi_0^N \rangle_{N-1}||^2 = \sum_i ||x_i^{(n)}||^2 \qquad (11)$$

In practice, at the ADC(3) level, the Feynman−Dyson transition amplitudes used to calculate the pole strengths (eq 11) or expand Dyson orbitals (eq 9) readily derive from the 1h and 1p components of the eigenvectors associated with the electron binding energies of interest.[13] In the sequel, the ADC(3) ionization energies and related Dyson orbitals have been used to simulate (e,2e) ionization spectra at specific azimuthal angles, using the convolution procedure described in the previous section (fwhm = 1.1 eV). To be more specific, in these simulations, line intensities for each identified states are scaled according to cross sections computed by means of eqs 5−7, thus from Dyson orbitals with a norm equal to the related spectroscopic strength, Γ_n.

Within the so-called target Kohn−Sham approximation,[1] one assumes that Dyson orbitals can be replaced by Kohn−Sham orbitals. In all analyses of EMS experiments so far, these at best derive from DFT calculations employing standard gradient-corrected and nonlocal hybrid exchange-correlation functionals, such as B3LYP. We would like to emphasize that this approximation is only empirical in nature, since no theory so far ever proved that a formal relationship exists between the Kohn−Sham and Dyson orbitals of a *correlated* system in its *neutral* ground state. To be more specific, Kohn−Sham orbitals are obviously not suited for coping with configuration interactions in the *cation*, and with a systematic and often extremely significant dispersion therefore[4,5] of the ionization intensity into a formally infinite[70] number of satellites. In addition, density functional theory (DFT) suffers from fundamental limitations, among which is the *incorrect behavior*[71] *of most currently used exchange-correlation potentials in the asymptotic region* ($r \to \infty$, $p \to 0$), due to the unavoidable self-interaction error. The latter error is known to yield systematic underestimations, by several electronvolts, of ionization energies.[3o,3p,5,72,73] Despite these fundamental limitations, Kohn−Sham orbitals are known in practice to provide amazingly accurate insights into experimentally determined electron momentum distributions,[3] possibly as the outcome of a compensation of several errors.[73]

Spherically averaged orbital momentum distributions have been generated from the output of 1p-GF/ADC(3) or DFT calculations using the MOMAP program by Brion and coworkers[74] and homemade interfaces. For comparison purposes, the most accurate ADC(3)/cc-pVDZ++ Dyson orbital distributions presented in the sequel have also been convolved by means of the Gaussian weighted planar grid (GW-PG) method of Duffy et al.,[75] according to an experimental electron momentum resolution of 0.1 au (fwhm). This value is consistent with an angular resolution of $\Delta\phi = 1.2°$ at a total impact energy of 1200 eV.[76]

In line with these calculations, (e,2e) ionization spectra can be easily simulated using the ADC(3) output and Dyson orbitals for all identified one-electron and shake-up lines. Specifically, in these simulations, line intensities are scaled according to (e,2e) ionization cross sections computed using eqs 5−7.

Results and Discussion

(a) Molecular Structures and Relative Conformer Energies. Presented in Table 1 are the main geometric parameters characterizing the C−O−C−O−C backbone of the four conformers of dimethoxymethane, TT, TG, G^+G^+, and G^+G^-, which were optimized at the B3LYP/aug-cc-pVTZ level under the constraints of the C_{2v}, C_1, C_2, and C_s symmetry point groups, respectively. In all four cases, vibrational analysis confirmed that these point groups are compatible with local energy minima, in line with the most thorough (B3LYP/6-31++G**) calculations available to date on this molecule.[22,23] Note that, without diffuse functions in the basis set, the G^+G^- conformer (C_s structure) is a first-order saddle point on the (B3LYP/cc-pVTZ) potential energy surface, most certainly due to an incomplete depiction of the through-space orbital interactions associated with the anomeric effect, and of the dispersion forces between the terminal methyl groups. This observation is consistent with earlier studies[29] performed with much smaller basis sets (4-31G, D95**, D95(2df,p)). For the latter species, at the B3LYP/aug-cc-pVTZ level, unusually large atomic displacements and low forces were experienced at the final stages of the geometry optimization process, which indicates that the associated energy minimum is a very shallow one. An extremely low vibrational frequency is correspondingly found for the G^+G^- conformer. Note that the TG conformer was obtained by optimizing at the

TABLE 1: Selected B3LYP/aug-cc-pVTZ Optimized Geometric Parameters for the Four Conformers of Dimethoxymethane[a]

TT Conformer (C_{2v}):
$C_1-O_1 = O_2-C_3 = 1.411$; $O_1-C_2 = C_2-O_2 = 1.395$
$\theta(C_1,O_1,C_2) = \theta(C_2,O_2,C_3) = 112.4$; $\theta(O_1,C_2,O_2) = 105.9$
$\varphi(C_1,O_1,C_2,O_2) = \varphi(O_1,C_2,O_2,C_3) = 180.0$

TG Conformer (C_1):
$C_1-O_1 = 1.423$; $O_1-C_2 = 1.383$; $C_2-O_2 = 1.415$; $O_2-C_3 = 1.414$
$\theta(C_1,O_1,C_2) = 114.4$; $\theta(O_1,C_2,O_2) = 110.1$; $\theta(C_2,O_2,C_3) = 112.7$
$\varphi(C_1,O_1,C_2,O_2) = 68.7$; $\varphi(O_1,C_2,O_2,C_3) = -178.5$

G^+G^+ Conformer (C_2):
$C_1-O_1 = O_2-C_3 = 1.422 = (\mathit{1.425 \pm 0.004})$[b]
$O_1-C_2 = C_2-O_2 = 1.403 = (\mathit{1.400 \pm 0.004})$[b]
$\theta(C_1,O_1,C_2) = \theta(C_2,O_2,C_3) = 114.0 = \mathit{112.9}$[b]
$\theta(O_1,C_2,O_2) = 114.1 = \mathit{113.7}$[b]
$\varphi(C_1,O_1,C_2,O_2) = \varphi(O_1,C_2,O_2,C_3) = 68.8 = \mathit{68.1}$[b]

G^+G^- Conformer (C_s):
$C_1-O_1 = O_2-C_3 = 1.419$; $O_1-C_2 = C_2-O_2 = 1.403$
$\theta(C_1,O_1,C_2) = \theta(C_2,O_2,C_3) = 116.9$; $\theta(O_1,C_2,O_2) = 115.6$
$\varphi(C_1,O_1,C_2,O_2) = -\varphi(O_1,C_2,O_2,C_3) = 84.8$

[a] Bond lengths are in angstroms. Bond (θ) and dihedral (φ) angles are in degrees. [b] Experimental X-ray diffraction data.[35]

same level a strongly asymmetric structure resembling the G^+G^- conformer of *n*-pentane,[45] with in the first step C−O−C−O and O−C−O−C dihedral angles equal to 63° and −90°.

In general, end C−O bonds are slightly longer, by ∼0.02 Å, than the central O−C bonds. The gauche segments of the TG, G^+G^+, and G^+G^- conformers are characterized by C−O−C bond angles ranging from 114° to 116°, as a result of unfavorable steric and electrostatic interactions between the CH_3 and CH_2 groups, and of the anomeric effect, which tends to drive the oxygen atoms toward an sp^2 state of hybridization. In straightforward analogy with *n*-pentane,[45] unusually large torsion angles, around ∼85°, are observed within the C−O−C−O−C backbone for the G^+G^- conformer of dimethoxymethane, as a result of particularly strong steric and electrostatic repulsion forces in this species.

For the G^+G^+ conformer, the computed C−O−C or O−C−O bond angles (114.0°, 114.1°), as well as the dihedral (O−C−O−C or C−O−C−O) angles (68.8°), compare rather favorably with available electron diffraction data (114.6 ± 0.5°, 114.3 ± 0.7°, and 63.3 ± 0.9° [33a]), or microwave rotational spectroscopic data, (111.4°, 112.8°, and 67.6°, respectively[36a]). See also Table 1 for a comparison of the calculated geometry for this conformer with recent X-ray diffraction data.[35] Our results are found to be in quantitative agreement with the latter data, despite possible complications due to temperature effects as well as intermolecular interactions in the solid state.

Results of the focal point analysis of the conformer energies of dimethoxymethane relative to the most stable form (G^+G^+) are given in Tables 2−4, which are formed by listing theoretical methods of improving quality on one axis, and basis sets of increasing size on the other, with the best result being obviously given by the entry at the lower right corner. From these tables, extremely accurate predictions of conformer energy differences can be made by pairing different levels of theory with various basis sets. To be more specific, the values reported under the ΔHF entry correspond to the conformational energy differences at the HF level, whereas the values reported in the +MP2, +MP3, +CCSD, and +CCSD(T) entries are the corrections to the conformational energy differences obtained by comparing successively the MP2 with the HF results, the MP3 with the MP2 results, the CCSD with the MP3 results, and, at last, the CCSD(T) with the CCSD results. In each column, the sum of the reported values up to a given row associated with a specific theoretical model gives thus the relative conformer energy for that model chemistry in particular.

The key point in a focal point analysis is to determine at which basis set each of the successive corrections evaluated by the various ab initio methods has converged. Very clearly, the most important corrections to the ΔHF results are the MP2 ones, the convergence of which is rather slow. At the HF and MP2 levels, diffuse functions have a very substantial influence on the computed energy differences, due to the through-bond and through-space orbital interactions associated with the anomeric effect. Therefore, comparing the ΔHF results and MP2 corrections obtained using the cc-pVQZ and aug-cc-pVQZ basis sets indicates near convergence for these quantities, within 0.2 kJ/mol, with respect to further improvements of the basis set. In contrast, a comparison with energy differences obtained using the aug-cc-pVTZ and cc-pVQZ basis sets indicates an almost complete convergence, within 0.02 kJ/mol, of the CCSD correction to the MP3 result. Similarly, comparing the CCSD(T)/aug-cc-pVDZ and CCSD(T)/aug-cc-pVTZ corrections to the CCSD result obtained with the same basis sets demonstrates the convergence of the +CCSD(T) correction within ∼0.04 kJ/mol.

In Tables 2−4, the values displayed in italics derive either from extrapolations to the limit of asymptotically complete basis sets, using the procedures by Feller or Schwarz (see Theory and Methodology), or from extrapolations employing our best estimates (in boldface) of the successive contributions and corrections to the relative conformer energies. Note that the most prohibitive MP3/aug-cc-pVQZ, CCSD/cc-pVQZ, and CCSD(T)/aug-cc-pVTZ calculations were so computationally demanding that the frozen core approximation has been used almost systematically, in order to make these calculations tractable. Within the framework of this approximation, a value of 10.93 kJ/mol is thus for instance found for the extrapolated CCSD(T)/aug-cc-pV∞Z energy of the TG conformer relative to the G^+G^+ global energy minimum, by adding to the ΔHF/aug-cc-pV∞Z result (7.67 kJ/mol) the best estimates (+3.34, −1.21, +0.51, and +0.61 kJ/mol) for the +MP2, +MP3, +CCSD, and +CCSD(T) corrections. The G^+G^- and TT rotamers are similarly located at relative energies of 15.98 and 23.72 kJ/mol.

Errors made because of the frozen core approximation upon the correlation corrections to the HF energy differences were estimated separately for all employed model chemistries, using the cc-pVDZ and cc-pVTZ basis sets, by comparing results obtained for these basis sets with and without using this approximation. The core level contributions to the successive correlation corrections to the computed energy differences are listed under the two rightmost entries of Tables 2−4. As is immediately apparent, the frozen core approximation has a very marginal effect, below ∼0.1 kJ/mol, on the computed energy differences. Accounting for these contributions leads to energy differences of 10.88, 16.08, and 23.64 kJ/mol between, on the one hand, the TG, G^+G^-, and TT conformers, and the G^+G^+ conformer on the other hand. The latter values thus define our best estimates, to be used in the forthcoming statistical thermodynamic study of the conformational equilibrium of dimethoxymethane, for the energy of the TG, G^+G^-, and TT species relative to that of the G^+G^+ global energy minimum form. Compared with these, the B3LYP/aug-cc-pVTZ energy differences (Table 5) are in error by ∼1.2 to ∼2.5 kJ/mol. For the sake of completeness, we provide in Table 5 internal energy (or enthalpy) differences at 0 K including

TABLE 2: Focal Point Analysis of the Energy of the TG Conformer of Dimethoxymethane Relative to the G^+G^+ Species[a]

basis	3-21G[b] (61 MOs)	cc-pVDZ[b] (110 MOs)	aug-cc-pVDZ[b] (187 MOs)	cc-pVTZ[b] (262 MOs)	aug-cc-pVTZ[b] (414 MOs)	cc-pVQZ[b] (515 MOs)	aug-cc-pVQZ[b] (768 MOs)	cc-pV∞Z[c]	aug-cc-pV∞Z[c]	cc-pcVDZ[d] (130 MOs)	cc-pcVTZ[d] (327 MOs)
ΔHF	19.23	10.40	8.30	8.42	7.95	7.86	7.79	*7.673*	***7.673***		
+MP2	1.628	2.673	3.643	2.978	3.436	3.169	3.360	*3.228*	***3.341***	0.063	**−0.026**
+MP3	−1.247	−1.235	−1.208	−1.241	−1.200	−1.220	−1.221	*−1.234*	***−1.208***	−0.016	**−0.015**
+CCSD	0.843	0.675	0.553	0.570	0.535	0.528		***0.512***		0.010	**−0.006**
+CCSD(T)	0.320	0.415	0.601	0.501	**0.607**					**0.003**	
total	20.777	12.933	11.890	11.225	11.331	*10.944*[e]	*11.062*[e]	*10.786*[e]	*10.925*[e]	*10.985*	*10.881*[f]

[a] Values given in italics refer to extrapolations; energies are expressed in kilojoules per mole. [b] Calculations employing the frozen core approximation. [c] HF energies are extrapolated according to a three-point Feller extrapolation; correlation energies are extrapolated according to a three-point Schwarz extrapolation (frozen core). [d] Frozen core−full correlation energy corrections are the differences between the corresponding frozen core and the full calculations. [e] Extrapolated values, using the best values on left for the missing corrections. [f] Best estimate, obtained by summing the HF/aug-cc-pV∞Z value and all corrections in boldface.

TABLE 3: Focal Point Analysis of the Energy of the G^+G^- Conformer of Dimethoxymethane Relative to the G^+G^+ Species[a]

basis	3-21G[b] (61 MOs)	cc-pVDZ[b] (110 MOs)	aug-cc-pVDZ[b] (187 MOs)	cc-pVTZ[b] (262 MOs)	aug-cc-pVTZ[b] (414 MOs)	cc-pVQZ[b] (515 MOs)	aug-cc-pVQZ[b] (768 MOs)	cc-pV∞Z[c]	aug-cc-pV∞Z[c]	cc-pcVDZ[d] (130 MOs)	cc-pcVTZ[d] (327 MOs)
ΔHF	22.97	20.69	18.04	18.42	17.73	17.75	17.59	*17.502*	***17.527***		
+MP2	−3.201	−0.766	−1.237	−1.263	−1.106	−1.113	−1.035	*−1.068*	***−1.005***	0.110	**0.112**
+MP3	0.120	−0.447	−0.411	−0.534	−0.368	−0.443	−0.377	*−0.455*	***−0.394***	−0.013	**−0.019**
+CCSD	0.152	0.202	0.173	0.268	0.228	0.262		***0.295***		0.001	**0.011**
+CCSD(T)	−0.607	−0.432	−0.402	−0.479	**−0.445**					**−0.004**	
Total	19.438	19.243	16.166	16.412	16.041	*16.010*[e]	*15.994*[e]	*15.830*[e]	*15.979*[e]	*16.073*	*16.080*[f]

[a] Values given in italics refer to extrapolations; energies are expressed in kilojoules per mole. [b] Calculations employing the frozen core approximation. [c] HF energies are extrapolated according to a three-point Feller extrapolation; correlation energies are extrapolated according to a three-point Schwarz extrapolation (frozen core). [d] Frozen core−full correlation energy corrections are the differences between the corresponding frozen core and the full calculations. [e] Extrapolated values, using the best values on left for the missing corrections. [f] Best estimate, obtained by summing the HF/aug-cc-pV∞Z value and all corrections in boldface.

TABLE 4: Focal Point Analysis of the Energy of the TT Conformer of Dimethoxymethane Relative to the G^+G^+ Species[a]

basis	3-21G[b] (61 MOs)	cc-pVDZ[b] (110 MOs)	aug-cc-pVDZ[b] (187 MOs)	cc-pVTZ[b] (262 MOs)	aug-cc-pVTZ[b] (414 MOs)	cc-pVQZ[b] (515 MOs)	aug-cc-pVQZ[b] (768 MOs)	cc-pV∞Z[c]	aug-cc-pV∞Z[c]	cc-pcVDZ[d] (130 MOs)	cc-pcVTZ[d] (327 MOs)
ΔHF	42.57	23.55	18.72	19.27	18.04	17.98	17.79	*17.484*	***17.652***		
+MP2	0.344	4.623	6.770	5.804	6.172	5.869	6.069	*5.907*	***6.037***	0.071	**−0.050**
+MP3	−1.792	−2.438	−2.436	−2.489	−2.335	−2.389	−2.348	−2.397	***−2.336***	−0.024	**−0.027**
+CCSD	1.737	1.476	1.212	1.239	1.178	1.154		***1.168***		0.023	**−0.021**
+CCSD(T)	0.468	0.810	1.184	1.088	**1.204**					**0.007**	
Total	43.324	28.025	25.450	24.914	24.256	*23.815*[e]	*23.865*[e]	*23.365*[e]	*23.724*[e]	*23.802*	*23.635*[f]

[a] Values given in italics refer to extrapolations; energies are expressed in kilojoules per mole. [b] Calculations employing the frozen core approximation. [c] HF energies are extrapolated according to a three-point Feller extrapolation; correlation energies are extrapolated according to a three-point Schwarz extrapolation (frozen core approximation). [d] Frozen core−full correlation energy corrections are the differences between the corresponding frozen core and the full calculations. [e] Extrapolated values, using the best values on left for the missing corrections. [f] Best estimate, obtained by summing the HF/aug-cc-pV∞Z value and all corrections in boldface.

TABLE 5: Evaluation of Relative Energy (or Enthalpy) Differences at Using the FPA Results of Tables 2−4 and the B3LYP/aug-cc-pVTZ Corrections for Zero-Point Harmonic Vibrational Energies ($\Delta H_0 = \Delta E$(FPA) + ΔZPVE)[a]

conformer	G^+G^+	TG	G^+G^-	TT
ΔE(FPA)[b]	0.000	10.881	16.080	23.635
ΔE[c]	0.000	9.459	14.763	21.132
ΔZPVE[c]	0.000	−0.934	−0.759	−2.124
ΔH_0	0.000	9.947	15.321	21.512

[a] All energy differences are given in kilojoules per mole. [b] Taken from the focal point analysis (see Tables 2−4). [c] Differences obtained from B3LYP/aug-cc-pVTZ calculations.

B3LYP/aug-cc-pVTZ corrections for zero-point vibrational energies (ZPVEs) [$\Delta H_0 = \Delta U_0 = \Delta E$(FPA) + ΔZPVE]. Considering that, compared with the latter contributions, thermal corrections to internal energies or enthalpies at room temperature are marginal, the ΔH_0 enthalpy difference that is found (9.95 kJ/mol) between the TG and G^+G^+ species appears to be fully consistent with a reported experimental value of 10.5 ± 0.8 kJ/mol, according to temperature-dependent NMR measurements of $^{13}C-^{1}H$ coupling constants in the gas phase.[34]

(b) Conformational Equilibrium. Along with the extremely accurate conformational energy differences derived from focal point analyses [ΔE(FPA)], we display in Table 6 the enthalpy corrections ($\Delta\Delta H_{298}$, including zero-point vibrational energies) obtained at room temperature from the B3LYP/aug-cc-pVTZ geometric and vibrational results for each of the conformers of interest, using Boltzmann statistical thermodynamics at the elementary RRHO level, as well as upon taking into account the influence of rigid-rotor hindered rotations, using the protocol by Ayala and Schlegel.[60] We correspondingly provide in this table our best estimates for the enthalpy, entropy, and Gibbs free energy differences, with and without accounting for the hindered rotations. It is immediately apparent from this table that hindered rotations, in particular those associated with the terminal methyl groups, have quantitatively a rather significant influence, on the order of ∼1.0 to ∼2.5 kJ/mol, on the obtained

TABLE 6: Evaluation, Using Boltzmann Statistical Thermodynamics at the Level of the Rigid Rotor−Harmonic Oscillator and upon Accounting for Hindered Rotations, of the Abundance of the Four Conformers of Dimethoxymethane at Room Temperature (T = 298.15 K), Using the Best FPA Estimates (Tables 2−4) for the Energy Differences, and the B3LYP/aug-cc-pVDZ Estimates for the Zero-Point Vibrational and Thermal Contributions to the Enthalpy Differences ($\Delta\Delta H_{298} = \Delta H_{298} - \Delta E$), for the Relative Enthalpies ($\Delta H_{298} = \Delta E$(FPA) + $\Delta\Delta H_{298}$), for Relative Entropies (ΔS_{298}), and for the Relative Gibbs Free Energies ($\Delta G_{298} = \Delta H_{298} - T\Delta S_{298}$)

	hindered rotations				RRHO			
	G^+G^+	TG	G^+G^-	TT	G^+G^+	TG	G^+G^-	TT
ΔE(FPA)[a]	0.000	10.881	16.080	23.635	0.000	10.881	16.080	23.635
$\Delta\Delta H_{298}$[a]	0.000	−0.602	−1.343	−1.741	0.000	−0.778	−0.331	−1.527
ΔH_{298}[a]	0.000	10.279	14.737	21.894	0.000	10.103	15.749	22.108
ΔS_{298}[b]	0.000	−1.197	14.707	8.996	0.000	7.146	21.920	5.761
ΔG_{298}[a]	0.000	10.635	10.352	19.212	0.000	7.974	9.214	20.390
abundance	0.9587	0.0263	0.0147	0.0002	0.9053	0.0726	0.0220	0.0001

[a] In kJ/mol. [b] In J/(K·mol).

TABLE 7: Evalution of the Conformer Distribution as a Function of the Temperature

temp (K)	G^+G^+ (C_2)	TG (C_1)	G^+G^- (C_s)	TT (C_{2v})
198.15	0.9958	0.0034	0.0007	0.0000
223.15	0.9912	0.0068	0.0020	0.0000
248.15	0.9837	0.0117	0.0045	0.0000
273.15	0.9730	0.0183	0.0086	0.0001
298.15	0.9588	0.0263	0.0147	0.0002
323.15	0.9411	0.0356	0.0229	0.0004
348.15	0.9205	0.0458	0.0329	0.0007
373.15	0.8973	0.0567	0.0448	0.0011
398.15	0.8721	0.0679	0.0583	0.0017

Gibbs free energy differences, mostly via the computed entropies. The effect is particularly pronounced for the TG conformer.

In line with the respective symmetry point groups, the symmetry numbers ρ_i to retain for evaluating the conformer abundance of each species via eq 3 have been set equal to 2, 4, 2, and 1 for the G^+G^+, TG, G^+G^-, and TT conformers, respectively. Accounting for hindered rotations results in minor variations, by ∼5%, in the computed abundances. According to our most exact model, only the G^+G^+ conformer contributes significantly, with a molar fraction approaching 0.96, to the conformational mixture characterizing a gas-phase sample of dimethoxymethane at 298 K. Conformer abundances have been similarly calculated at other temperatures (Table 7), using in each case vibrational and rotational partition functions accounting for hindered rotations. It is only at temperatures above 100 °C that the molar fractions of the TG and G^+G^- conformers exceed 5%, and may then become significant from a spectroscopic viewpoint. Note that the weight of the TT conformer remains totally negligible, whatever the considered temperature or the level of theory reached for the thermodynamic calculations. This rotamer may therefore clearly be regarded as an "electrostatically forbidden" structure.

Considering the results of our focal point analysis and thermodynamic calculations, as well as the still rather limited energy resolution and signal-to-noise ratio of the best (e,2e) spectrometers that are currently available, it is therefore a very reasonable choice to predict the results of EMS experiments on dimethoxymethane from calculations on the G^+G^+ conformer alone.

(c)Valence Electronic Structure and Ionization Spectra. The spike and convoluted ADC(3) spectra displayed in Figure 2 reflect the partition of the valence electronic structure of dimethoxymethane into 5 inner-valence levels (O_{2s}, C_{2s}) and 11 outer-valence levels (O_{2p}, C_{2p}, H_{1s}), at electron binding energies above and below ∼19 eV, respectively. At the HF/aug-cc-pVTZ level, the most stable G^+G^+ conformer of dimethoxymethane in its (X^1A) ground state has, under the constraint of a C_2 symmetry point group, the following inner and outer valence shell electronic configurations:

inner-valence shell: $\{(4a)^2\,(3b)^2\,(5a)^2\,(4b)^2\,(6a)^2\}$

outer-valence shell:
$$\{(5b)^2\,(7a)^2\,(6b)^2\,(8a)^2\,(7b)^2\,(9a)^2\,(8b)^2\,(10a)^2\,(9b)^2\,(11a)^2\,(10b)^2\}$$

The corresponding molecular orbitals are displayed in Figure 3. The two innermost orbitals (4a, 3b) giving rise to the bands at ∼32 and ∼34 eV in the ADC(3)/cc-pVDZ spectrum (Figure 2c, Table 8) relate merely to bonding and antibonding combinations of O_{2s} atomic orbitals. Analysis of the LCAO eigenvectors indicates that the next three orbitals (5a, 4b, 6a) are dominated by C_{2s} contributions. Admixture of C_{2p} and H_{1s} contributions is nonetheless noted (Figure 3) for the orbital (6a) at the top of the inner-valence region, which through-space interactions between σ orbitals associated with C−H bonds help to slightly stabilize. The first orbital (5b) in the outer-valence region exhibits correspondingly a significant C2s character. Such mixtures of C_{2s} and C_{2p} + H_{1s} contributions across the gap separating the inner- and outer-valence regions is a very typical consequence of through-space methylenic hyperconjugation effects.[77] Running further toward lower binding energies, the next seven orbitals that we encounter (5b, 6b, 7a, 8a, 7b, 9a, 8b) merely derive from combinations of C_{2p} and H_{1s} orbitals. Upon analyzing the LCAO eigenvectors, the molecular orbitals that dominantly relate to the four oxygen lone pairs are, clearly, the four outermost ones (10b, 11a, 9b, 10a). The two highest-lying canonical orbitals (10b and 11a) defining the HOMO (highest occupied molecular orbital) and HOMO − 1 levels derive essentially from linear combinations of two localized n_π-(2p)-type oxygen lone pairs, with no or limited through-bond interaction via the $\pi(CH_2)$ orbitals (Figure 3). In contrast, the next two highest-lying occupied orbitals (9b, 10a) describe (Figure 3) delocalization of the two remaining $n_\sigma(sp^2)$-type oxygen lone pairs over the vicinal C−O bonds and mixture with σ(C−O) and $\pi(CH_2)$ orbitals resulting in particularly favorable through-bond and through-space interactions along the C−O−C−O−C backbone. This orbital mixture can thus be typically regarded as the main outcome of the anomeric effect in a canonical (i.e., nonlocalized) depiction of the valence electronic structure of dimethoxymethane in its G^+G^+ conformation.

The reader is referred to Table 8 for an assignment of the He I photoelectron spectrum by Jørgensen et al. (Figure 2a),[38] through a confrontation with the available HF, DFT, and ADC-(3) data. It is immediately apparent that the ADC(3) calculations

TABLE 8: Assignment of the Experimentally Available Ionization Spectra of Dimethoxymethane, Using HF, DFT/B3LYP, and ADC(3) Ionization Energies[a]

band[b]	level	MO	HF/ aug-cc-pVDZ	B3LYP/ cc-pVDZ	B3LYP/ aug-cc-pVDZ	B3LYP/ aug-cc-pVTZ	ADC(3)/ cc-pVDZ	ADC(3)/ cc-pVDZ++	PES[c]	EMS[d]
I[e]	1	10b	12.029	7.257	7.583	7.627	10.331 (0.906)	10.608 (0.904)	10.29	10.41
	2	11a	12.053	7.415	7.735	7.771	10.490 (0.908)	10.756 (0.905)	10.53	
II[e]	3	9b	12.640	8.185	8.504	8.519	11.308 (0.910)	11.586 (0.906)	11.44	11.6[h]
III[e]	4	10a	14.203	9.616	9.897	9.905	12.942 (0.908)	13.177 (0.906)	12.98	13.2[h]
	5	8b	14.430	10.279	10.450	10.460	13.502 (0.914)	13.657 (0.911)	13.42	
IV[e]	6	9a	15.641	11.235	11.470	11.474	14.464 (0.907)	14.693 (0.903)	14.7[h]	15.2[h]
	7	7b	16.385	11.641	11.831	11.853	15.090 (0.905)	15.240 (0.902)	15.0[h]	
	8	8a	16.603	11.848	12.050	12.062	15.312 (0.905)	15.477 (0.902)		
V[e]	9	6b	**18.340**	13.508	13.764	13.761	**16.941** (0.894)	**17.193** (0.890)	16.9[h]	17.2[h]
	10	7a	**18.747**	13.453	13.699	13.698	**17.032** (0.889)	**17.250** (0.886)		
	11	5b	18.826	13.718	13.953	13.944	17.237 (0.894)	17.441 (0.890)		
VI	12	6a	22.859	16.607	16.805	16.784	20.663 (0.847)	20.807 (0.839)		20.6[h]
VII	13	4b[f,g]	25.369	18.744	18.941	18.902	22.778 (0.438)	22.884 (0.214)		
							22.790 (0.300)	22.929 (0.500)		
VIII	14	5a[f,g]	26.689	19.906	20.121	20.065	23.688 (0.117)	23.620 (0.026)		23.5[h]
							23.767 (0.137)	23.880 (0.141)		
							23.912 (0.160)	24.011 (0.120)		
								24.303 (0.101)		
IX	15	3b[f,g]	36.589	27.375	27.697	27.605	31.718 (0.031)	31.734 (0.011)		
							31.944 (0.064)	32.113 (0.011)		28−36[h]
X	16	4a[f,g]	38.433	28.977	29.291	29.196	33.167 (0.029)			
							34.096 (0.028)			

[a]Spectroscopic strengths (or pole strengths Γ_n) are given in parentheses. [b] The borders of peaks are based on ADC(3)/cc-pVDZ grounds. [c] See ref 38. [d] See ref 6. [e]These peaks reproducing the PES measurements are simulated using a spread Voigt function with an fwhm parameter of 0.6 eV (see Figure 2). [f] Breakdown of the orbital picture of ionization. Additional ADC(3)/cc-pVDZ shake-up lines: 4b (**13**): 22.916 (0.012), 23.891 (0.012); 5a (**14**): 23.514 (0.012), 23.971 (0.075), 24.007 (0.093), 24.228 (0.011), 24.281 (0.039), 24.414 (0.009), 24.451 (0.037), 24.493 (0.015), 24.680 (0.011), 24.859 (0.008), 24.919 (0.015), 25.111 (0.015); 3b (**15**): 31.067 (0.009), 31.140 (0.014), 31.279 (0.010), 31.294 (0.009), 31.457 (0.016), 31.496 (0.009), 31.596 (0.013), 31.632 (0.014); 31.739 (0.029), 31.868 (0.018), 31.912 (0.009), 31.947 (0.012), 32.062 (0.010), 32.180 (0.009), 32.227 (0.010), 32.273 (0.016), 32.281 (0.020), 32.443 (0.018), 32.508 (0.012); 4a (**16**): 32.195 (0.009), 32.295 (0.009), 32.522 (0.015), 32.809 (0.013), 33.096 (0.012), 33.346 (0.009), 33.827 (0.009), 34.053 (0.021), 34.099 (0.021), 34.136 (0.009), 34.190 (0.009), 34.268 (0.009), 34.314 (0.015), 34.334 (0.010), 34.363 (0.015). Breakdown of the orbital picture of ionization. Additional ADC(3)/cc-pVDZ++ shake-up lines: 6a (**12**): 21.287 (0.006), 22.233 (0.005); 4b (**13**): 23.083 (0.022), 23.636 (0.014), 24.026 (0.008); 5a (14): 23.676 (0.007), 23.738 (0.017), 23.766 (0.005), 23.820 (0.019), 23.993 (0.010), 24.068 (0.065), 24.100 (0.086), 24.148 (0.012), 24.201 (0.023), 24.317 (0.017), 24.415 (0.017), 24.576 (0.015), 24.629 (0.007), 24.736 (0.006), 24.788 (0.016), 24.830 (0.008), 24.849 (0.006), 24.944 (0.009), 24.999 (0.025); 3b (**15**) 31.949 (0.008), 32.064 (0.010), 32.167 (0.011), 32.182 (0.008), 32.195 (0.009), 32.264 (0.008),32.267 (0.010). [g] The total fraction of ionization intensity recovered at these binding energies for the 4b orbital is, at the ADC(3)/cc-pVDZ and ADC(3)/cc-pVDZ++ levels, equal to 0.762 and 0.760, respectively. For the 5a orbital this sum is correspondingly equal to 0.754 or 0.758, respectively. A major part of the missing fraction is expected to be found at higher electron binding energies.[70] [h] Own assignment.

enable quantitative insights, within ~0.3 eV, into the experimental one-electron binding energies. In contrast, it is clear that neither HF nor Kohn−Sham (KS) orbital energies provide reliable estimates of the experimentally obtained one-electron binding energies. Nonetheless, the ADC(3) results confirm that the order of ionization energies predicted from the HF or KS orbital energies is correct, up to the top of the inner-valence region at ~21 eV.

The obtained HF orbital binding energies overestimate the measured orbital ionization energies by 1.0−2.7 eV due to the neglect of electron relaxation and correlation effects. In line with a pioneering second-order Green's function study of the X-ray photoionization spectra of finite oligomer chains converging to polyoxymethylene,[77d] a comparison of the HF and ADC(3) results indicate that the relaxation effects are particularly pronounced for the two outermost orbitals (10b, 11a) relating to the two n_π(2p)-type oxygen lone pairs (Figure 3), and more limited for the deeper-lying n_σ(sp^2)-type oxygen lone pairs, because of the greater delocalization of the latter two levels. In contrast with the HF level, all KS orbital energies calculated by the B3LYP functional underestimate the experimental ionization energies by ~3 to ~4 eV. Such severe underestimations are most common with standard exchange-correlation (XC) functionals, essentially because of the too fast decay of the electronic potential at large *r*. Also, the equivalent of Koopmans' theorem in density functional theory (Janak's theorem[78]) only strictly holds for the highest occupied molecular orbital (HOMO). Despite the so-called meta-Koopman's theorem[79] that relates Kohn−Sham orbital energies to *relaxed* ionization energies, we would like to remind the reader, again, that the DFT formalism does not *explicitly* account for final-state configuration interactions leading to the dispersion of the ionization intensity into shake-up processes. At best, the DFT formalism can only *implicitly* account for electronic correlation and relaxation effects, *within the framework of a one-electron (or quasi-particle) picture of ionization*, through a *mapping of Kohn−Sham orbitals onto Dyson orbitals*. The B3LYP functional was certainly not designed to ensure such a mapping. The relationships between standard KS orbitals and ionization processes should therefore always be exploited with the greatest caution (see below).

At the 1p-GF/ADC(3) level, inclusion of diffuse functions results in shifts of the one-electron ionization energies by 0.15−0.28 eV toward higher electron binding energies (Table 8). The four lone-pair levels at binding energies comprised between 10.6 and 13.2 eV exhibit the strongest dependence on such improvements of the basis set. The most important shift is in particular observed for the line relating to orbital 9b. Similar observations can be made with the B3LYP Kohn−Sham orbital energies. It is worth noting that the calculated pole strengths remain almost constant ($\Gamma_n \sim 0.90 \pm 0.01$) within the outer-valence region (10−18 eV), and indicate that ionization processes at binding energies comprised between 10 and 18 eV are qualitatively correctly described by the removal of one electron from a

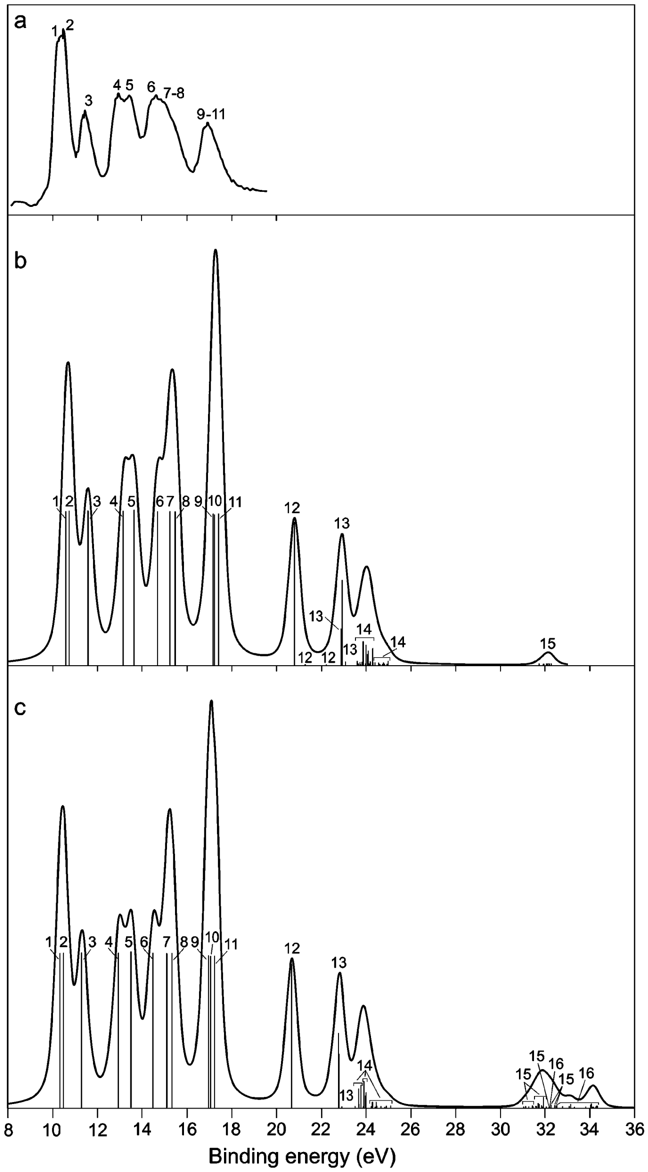

Figure 2. Comparison between (a) He I photoelectron spectra of dimethoxymethane obtained by Jørgensen[38] and theoretical ADC(3) spectra obtained using the (b) cc-pVDZ++ and (c) cc-pVDZ basis sets (convolution performed using a fwhm parameter of 0.6 eV).

specific molecular orbital. In contrast with our work on 1,3-butadiene,[18] for which intense shake-up lines were observed among the outermost π-ionization lines, these observations justify a comparison of the *shape* of KS orbital momentum distributions with that derived from *normalized* ADC(3) Dyson orbitals (eq 9) up to the upper edge of the inner-valence region, and a little beyond. The orbital picture of ionization remains indeed also essentially valid for the 6a level at ~20.8 eV (Γ_n = 0.84), and to a lesser extent for the 4b level at 22.9 eV (Γ_n = 0.50). This observation provides very strong support for earlier studies[77d,80] of conformational fingerprints at the top of the C_{2s} inner-valence bands of polyethers, due to hyperconjugation effects.

In contrast with the outer-valence region and latter two levels, both the ADC(3)/cc-pVDZ and ADC(3)/cc-pVDZ++ results point out a complete breakdown of the orbital picture of ionization for the three innermost valence orbitals (5a, 3b, and 4a), in the form of a severe dispersion of the ionization intensity over many lines with extremely limited strength, from which no clearly dominant 1h state emerges. In view of the simulations displayed in Figure 2, particularly broad bands are therefore expected at binding energies around ~24, ~32, and ~34 eV.

According to a comparison of energies obtained from single-point CCSD(T)/cc-pVDZ calculations upon the neutral and dication, the vertical double ionization threshold of dimethoxymethane in its G^+G^+ conformation lies at ~26.4 eV. All the 2h-1p shake-up states identified above that threshold should thus rather be regarded as approximations to unbound states that lie in the continuum and are thus subject to decay via emission of a second electron. In other words, the identified shake-up states above the double ionization threshold are approximations to *shake-off* resonances. Such states are extremely sensitive to improvements of the basis set, in particular to the inclusion of diffuse functions. This leads to a redistribution of the shake-up ionization intensity over many more lines, of which only a very marginal fraction can be recovered in the present work via the block-Davidson diagonalization procedure, due to the restriction of the search to lines with a pole strength larger than 0.005. These observations, and likely vibrational complications upon the sudden removal of two electrons, explain the extremely large width (~6 eV) observed for the O_{2s} band in the X-ray photoelectron spectra of polyoxymethylene, which HF orbital energies[80] or second-order quasi-particle Green's function ionization energies failed to explain.[77d] A very broad O_{2s} band, extending from ~28 to ~36 eV and possibly beyond, is also seen in the EMS ionization spectra recorded by Neville et al.[6] on dimethoxymethane (Figure 4).

Prior to proceeding to detailed calculations of electron momentum distributions, it is worth considering simulations (Figures 4 and 5) of ionization spectra obtained through EMS experiments upon the G^+G^+ conformer of dimethoxymethane at various azimuthal angles, in order to reliably identify the bands that are best suited for "orbital imaging" the anomeric effect and conformational fingerprints, despite the limited energy resolution reached with such experiments. The simulations displayed for various values of the out-of-plane scattering angle indicate that, at the larger azimuthal angles, five bands (I−V) can be reliably resolved in the outer-valence region of dimethoxymethane. The 6a level (6a) fingerprinting methylenic hyperconjugation[77d] can be individually resolved at all angles, in the form of a very sharp and intense peak at the top of the inner-valence region, around 20.8 eV. The deeper-lying C_{2s} and O_{2s} levels cannot be individually resolved, but rather yield broad signals in the experimental spectra, due to the shake-up fragmentation. To be more specific, the band observed at ~23.0 eV in the EMS measurements by Neville et al.[6] relates to a complex set of shake-up lines originating from the 4b and 5a inner-valence (C_{2s}) orbitals, whereas the very broad and intense band at binding energies comprised between 28 and 36 eV is ascribed to shake-off states associated with ionization of the innermost (O_{2s}) valence levels.

Because of unfavorable (e,2e) intensities reflecting a p-type electron momentum distribution, some bands (bands II, V, and VII) tend to disappear when the azimuthal angle vanishes. These conclusions corroborate the scheme proposed by Neville et al.[6] for deconvolving their (e,2e) ionization spectra recorded at an impact energy of 1200 eV under an estimated experimental energy resolution of 1.4 eV (fwhm), using the He I estimates of one-electron binding energies for locating the bands and Gaussian functions of varying width for optimizing the fit (Figure 4a,c).[75] Based on these simulations and on the band partition by Neville et al., we propose to pursue the discussion of the one-electron ionization bands of dimethoxymethane through simulations of electron momentum distributions for the

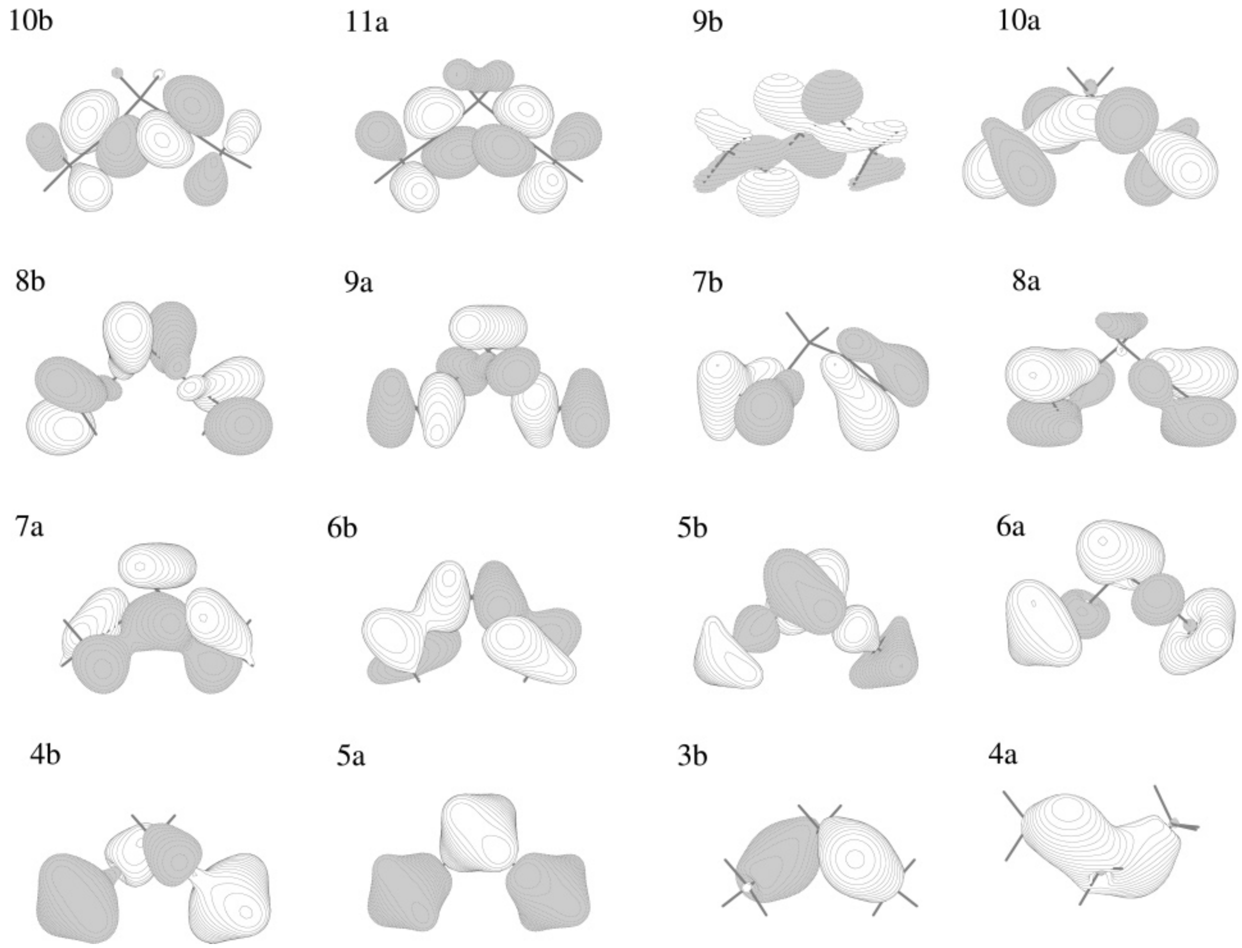

Figure 3. Valence molecular orbitals of the G^+G^+ conformer of dimethoxymethane (B3LYP/aug-cc-pVTZ results, using contour values equal to 0.05).

{10b + 11a}, {9b}, {10a + 8b}, {9a + 7b + 8a}, {6b + 7a + 5b} and {6a} sets of orbitals, ascribed to bands I, II, III, IV, V, and VI, respectively (Table 8). Due to a rather pronounced overlap with the HOMO, the case of orbital 9b relating to band II may be considered rather problematic, since Neville et al. might have gone beyond the limitations due to the low-energy resolution (1.4 eV) of their spectrometer.[6] According to our best calculations and simulations, the 9b orbital lies indeed at ~0.8 eV below the 11a orbital. The corresponding one-electron ionization line emerges nonetheless in the form of a distinct shoulder at ~11.6 eV in the simulation of Figure 4d (fwhm = 1.1 eV), an observation that should hopefully stimulate further EMS studies of dimethoxymethane at improved energy resolutions.

The simulated (e,2e) ionization spectra derived from ADC(3)/cc-pVDZ and ADC(3)/cc-pVDZ++ calculations are displayed as dashed and solid lines, respectively (see Figures 4 and 5). Upon examining these figures in detail, it is immediately apparent that our ADC(3)/cc-pVDZ++ simulations are overall in excellent agreement with the available experimental (e,2e) ionization spectra at $\phi = 0°$ and 9°, which confirms the high quality of the computed ionization energies and cross sections, and demonstrates the relevance of our theoretical analysis so far. It appears that, at large azimuthal angles, diffuse functions have only a moderate impact on the shape and relative intensities of bands. In sharp contrast, it is found that, at $\phi = 0°$, the inclusion of diffuse functions in the basis set yields a very strong rise of the (e,2e) ionization intensity characterizing band III at ~13.2 eV encompassing the 10a and 8b ionization channels. By virtue of the confrontation with experiment, this rise may be regarded as rather direct and irrefutable spectroscopic evidence for the through-space interactions governing the anomeric effect in dimethoxymethane, according to a canonical depiction of the valence electronic structure of this compound. Indeed, this rise is specifically ascribable to the 10a orbital, an ideally delocalized molecular orbital which describes (Figure 3) through-space and through-bond in-phase interactions between the $n_\sigma(sp^2)$-type oxygen lone pairs via the vicinal C−O bonds. Diffuse functions are obviously required for reliably describing such interactions and orbital mixings at large molecular distances ($r \to \infty$) and, thus, vanishing electron momenta ($p \to 0$). Further detailed experimental studies of the electron momentum densities associated with the 10a ionization channel are therefore very strongly encouraged.

(d) Electron Momentum Profiles. Electron momentum distributions for the six identified one-electron valence bands are displayed at various theoretical levels in Figures 6−11. The distribution of the area of peak I in the EMS ionization spectra of Neville et al. (Figure 4a,c) yields, after a conversion of the azimuthal angles ϕ into electron momenta, the experimental momentum density profiles displayed in Figure 6 (top) for the two outermost ionization lines. In each figure, we also display electron momentum distributions for the individual orbital levels. By analogy with atomic orbitals, these profiles can be roughly divided, depending on their symmetry, into two types of electron momentum distributions, referred to as s-type or p-type profiles. In the former case, molecular orbitals belonging to the symmetric representation (a) of the C_2 point group are all characterized by nonvanishing momentum density, i.e., (e,2e) ionization intensity at $p \sim 0$ a.u. ($\phi = 0°$), which tends to vanish at larger

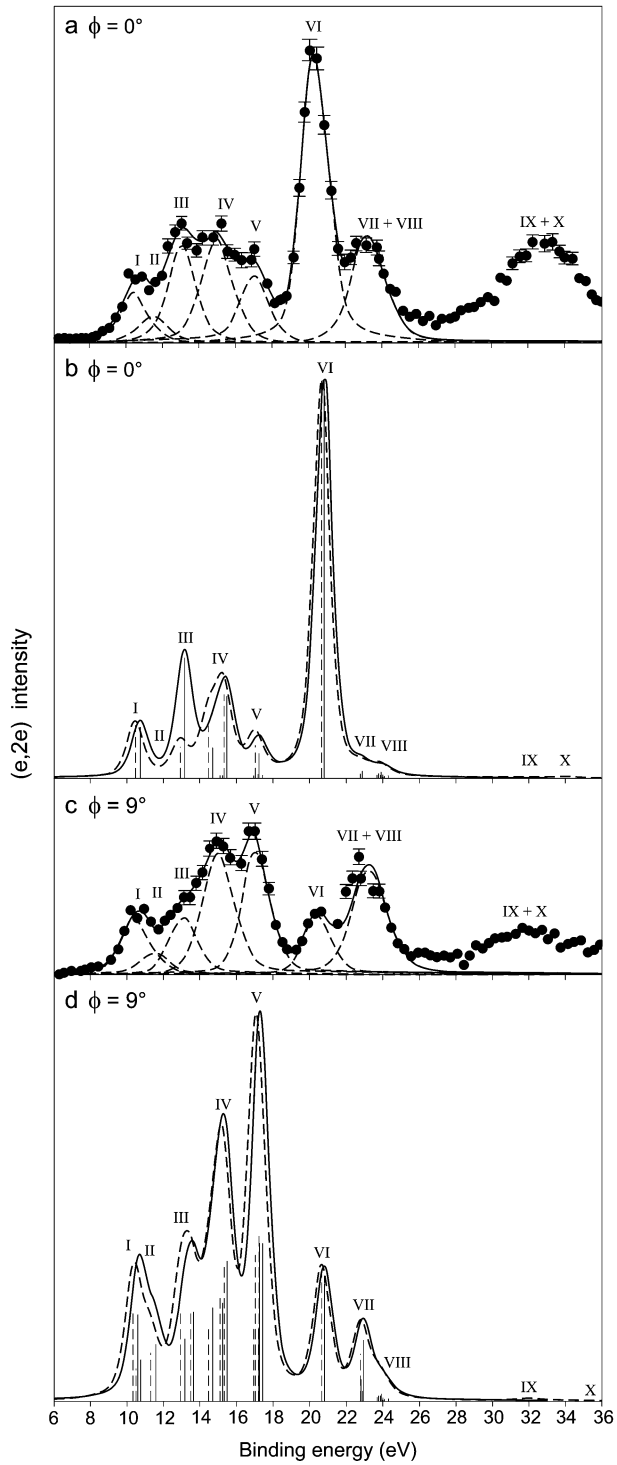

Figure 4. Comparison of (e,2e) experimental electron binding energy spectra recorded at azimuthal angles $\phi = 0°$ and 9° with theoretical simulations (dashed lines, ADC(3)/cc-pVDZ results; solid lines, ADC(3)/cc-pVDZ++ results).

electron momentum (azimuthal angles). In contrast, antisymmetric (b-type) molecular orbitals produce p-type profiles characterized by vanishing momentum density at $p \sim 0$. The contribution of the latter orbitals to (e,2e) ionization intensities gradually reaches a maximum at larger azimuthal angles.

Upon examining Figures 6−11, one may reasonably conclude that B3LYP Kohn−Sham orbitals and normalized ADC(3) Dyson orbitals for one-electron ionization bands provide overall qualitatively similar electron momentum distributions. The match is far from being always perfect, however, which leads us to call into question the assertion[79b] that the overlap between normalized Dyson and Kohn−Sham orbitals is most generally very close to 1. The latter statement was drawn from MRSDCI (multireference single double configuration interaction) calculations of Dyson orbitals for diatomic or triatomic molecules (CO, SiO, N_2, P_2, HF, HCl, H_2O, HCN, FCN). Due to the high symmetry point group of most of these molecules, significant alterations of overlap densities due to configurations interactions in the initial and final states are very unlikely. In contrast, the structure on which the present section focuses exhibits a very limited symmetry point group (C_2) that allows many more possibilities for orbital mixing and configuration interactions in the initial and final states. Quantitatively significant differences between Kohn−Sham and normalized ADC(3) Dyson orbital distributions are in particular observed (Figures 6−8) for the n_π(2p)-type and n_σ(sp^2)-type oxygen lone-pair levels (10b, 10a), due to the strength of electron pair relaxation (PRX) and electron pair removal (PRM) effects,[48,77d,82] and, in the latter case, through-space hyperconjugation interactions. In line with the intricate nodal structure of the related orbitals, indicating strong atomic orbital mixing, particularly strong differences are also found within the $C_{2p} + H_{1s}$ outer-valence bands for the 9a + 7b + 8a levels (Figure 9), defining the fourth set of lines at electron binding energies around ∼15 eV.

In many cases, and in particular at the lower electron binding energies, diffuse functions are also found to have an extremely substantial influence on the computed electron momentum profiles. It is worth noticing that the influence of diffuse functions on the calculated s-type electron momentum densities at the origin of momentum space is generally much more limited with the Kohn−Sham momentum distributions, which seems to be a rather obvious consequence of the too fast decay of the B3LYP electronic potential at large distances. Recalling that the cc-pVDZ++ basis set includes s-type and p-type diffuse functions derived from the aug-cc-pVDZ basis set, we also find that B3LYP/aug-cc-pVDZ and B3LYP/aug-cc-pVTZ momentum distributions are all almost identical, which makes us believe that the momentum distributions associated with the ADC(3)/cc-pVDZ++ Dyson orbitals should also be close to convergence with respect to further improvements of the basis set. Figures 6−11 also provide evidence for the rather substantial influence of the limited momentum resolution (0.1 au) of standard (e,2e) spectrometers on the apparent orbital shapes and spreads. The main outcome of resolution folding is overall a smoothing and flattening of the ADC(3)/cc-pVDZ++ momentum density profiles, in the form of a transfer of the (e,2e) ionization intensity from maxima to minima in the momentum distributions. The effect is particularly pronounced for orbitals 10b, 9b, 9a, and 6b (Figures 6, 7, 9, and 10, respectively). For these levels, it is comparable to the influence of the basis set and/or correlation treatment.

In agreement with experiment, the model predicts a mixed s−p-type momentum profile for the outermost band (I) at ∼10.4 eV (Figure 6). Such a profile is very typical of a set of lines comprising one symmetric orbital (11a) and one asymmetric orbital (10b). Compared with the B3LYP/aug-cc-pVDZ or B3LYP/aug-cc-pVTZ results, the ADC(3)/cc-pVDZ++ theoretical momentum distribution provides a slightly superior description of the relative intensity and position of the two maxima seen in the measured distribution. Indeed, at the B3LYP level, the extremum at $p \sim 0$ au is found to exhibit the largest (e,2e) cross sections at the B3LYP level, whereas the largest (e,2e) cross sections are seen for the extremum at $p \sim 0.88$ au and $p \sim 0.73$ au in the ADC(3) simulations and in the most

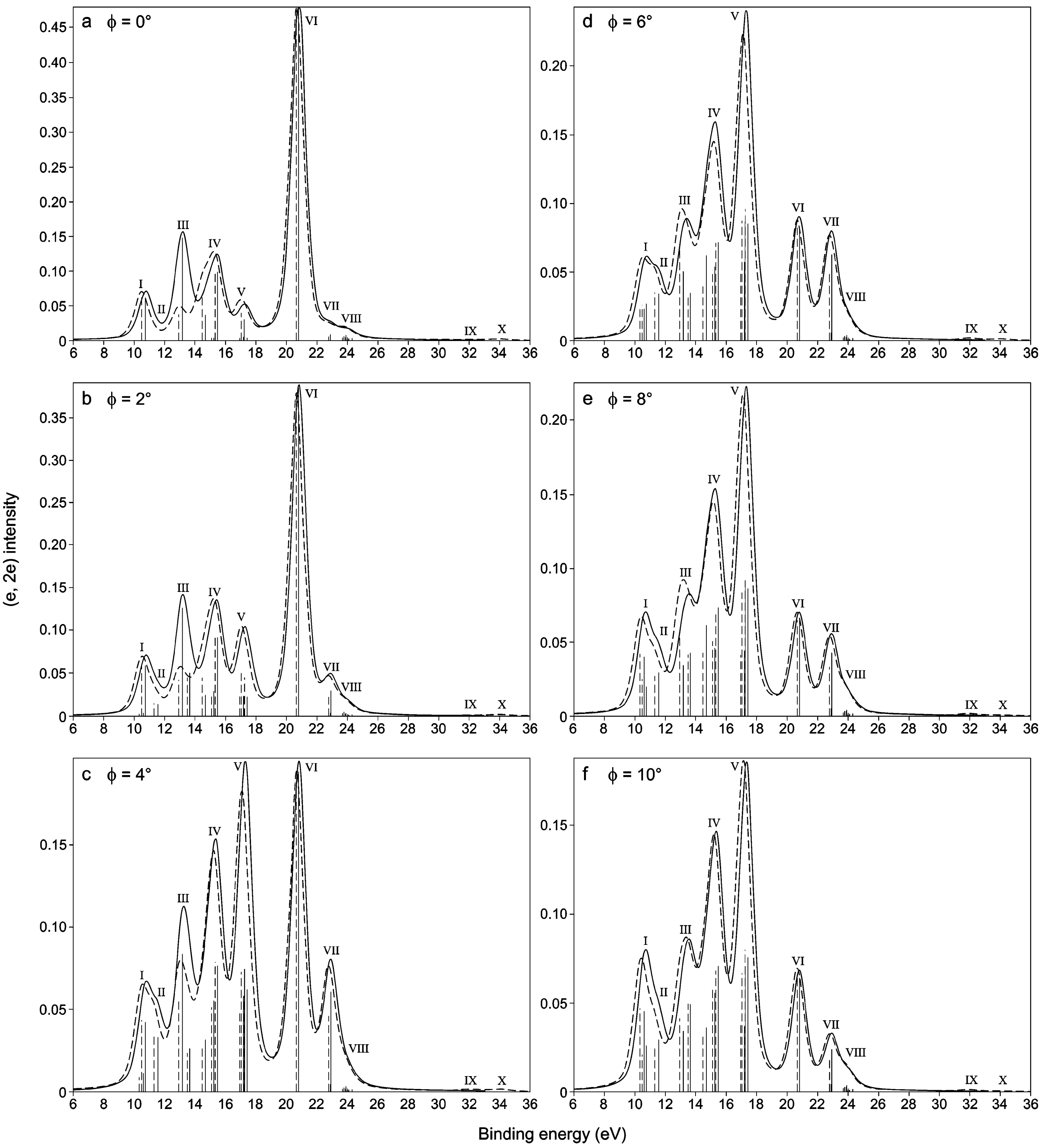

Figure 5. ADC(3) simulation of the dependence of the (e,2e) ionization spectrum of dimethoxymethane (G^+G^+ conformer only, fwhm = 1.1 eV). Solid and dashed lines or curves refer to results obtained using the cc-pVDZ++ and cc-pVDZ basis sets.

reliable (multichannel) measurements by Neville et al., respectively. For these levels, the KS momentum densities at nonvanishing momenta are more sensitive to the inclusion of diffuse functions than the Dyson counterpart. A shoulder at $p \sim 1.49$ au also characterizes the 10b theoretical momentum distribution, whereas for the 11a one a maximum is found at $p \sim 1.08$ au. Taking into account the randomization of (e,2e) ionization cross sections over all molecular orientations, these additional features reflect in both cases further confinements of the electron density at small values of r by several nodal surfaces across or along the O−C(H_3) bonds, in agreement with the molecular orbital topologies of Figure 3.

The EMS momentum distribution related to band II and orbital 9b at ~11.3 eV (Figure 7) is a p-type profile characterized by two main components at $p \sim 0.43$ au and $p \sim 1.17$ au. Here, again, the enhancement of the electron densities at large electron momenta reflects the presence of multiple nodal surfaces across the C−O−C−O−C backbone. The effect of the confinement is more limited when diffuse functions are incorporated in the basis set. Indeed, two sharp maxima are seen in the 9b momentum distributions computed using the cc-pVDZ basis set, whereas a broad shoulder is seen at $p \sim 1.0$ au in the profiles predicted at the ADC(3)/cc-pVDZ++ or B3LYP/aug-cc-pVTZ levels.

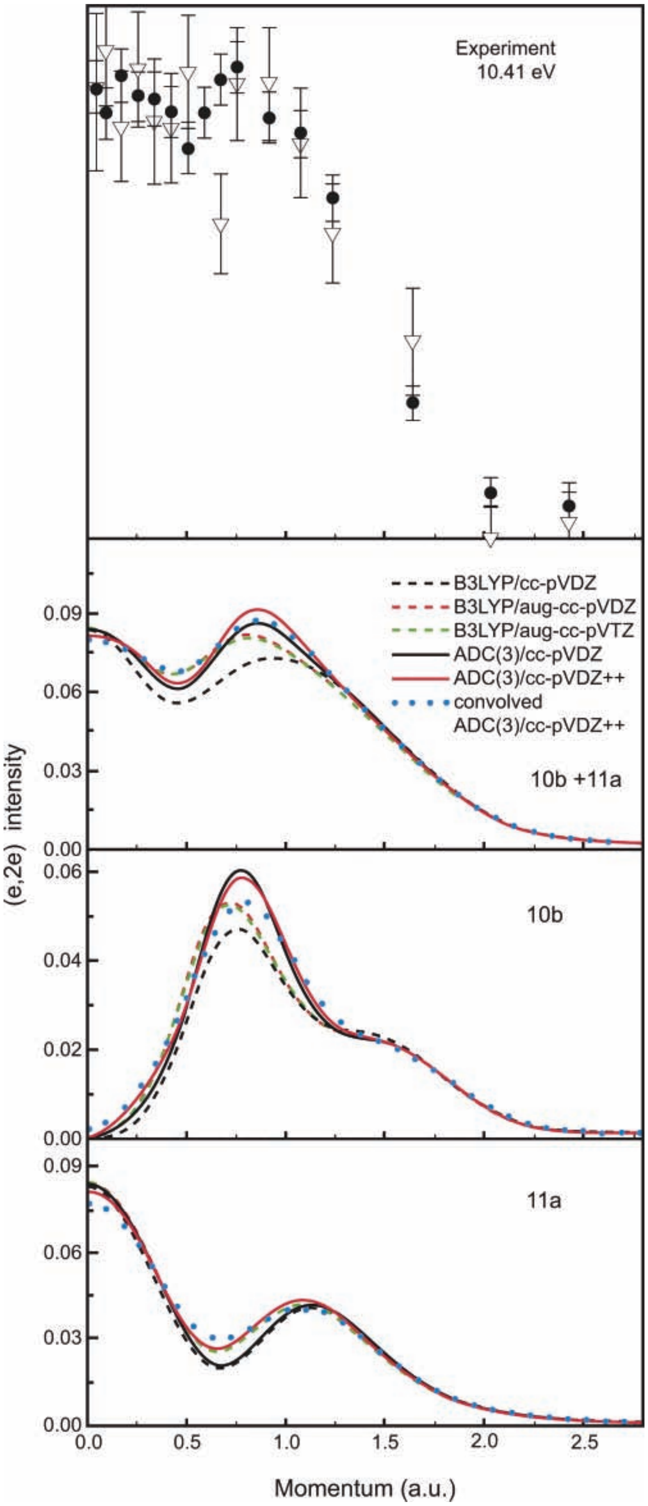

Figure 6. Experimental[6] and theoretical electron momentum distributions associated with band I at 10.41 eV. In the experimental part (top), the open triangles and solid dots are the momentum distributions inferred from single- and multiple-channel measurements by Neville et al.,[6] respectively.

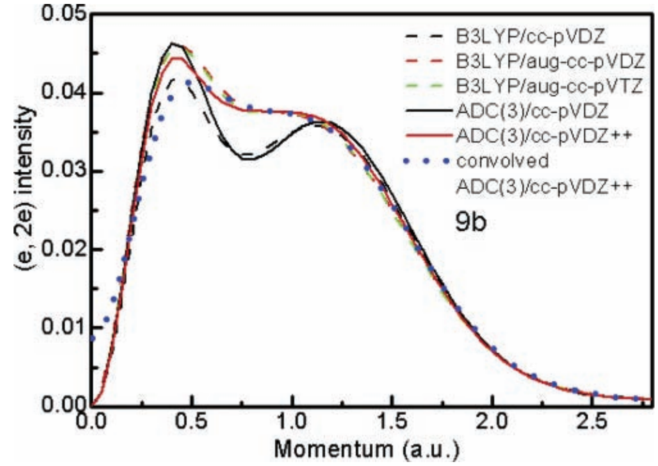

Figure 7. Dyson [ADC(3)] orbital and Kohn−Sham [B3LYP] orbital momentum distributions for orbital 9b, which resides under band II.

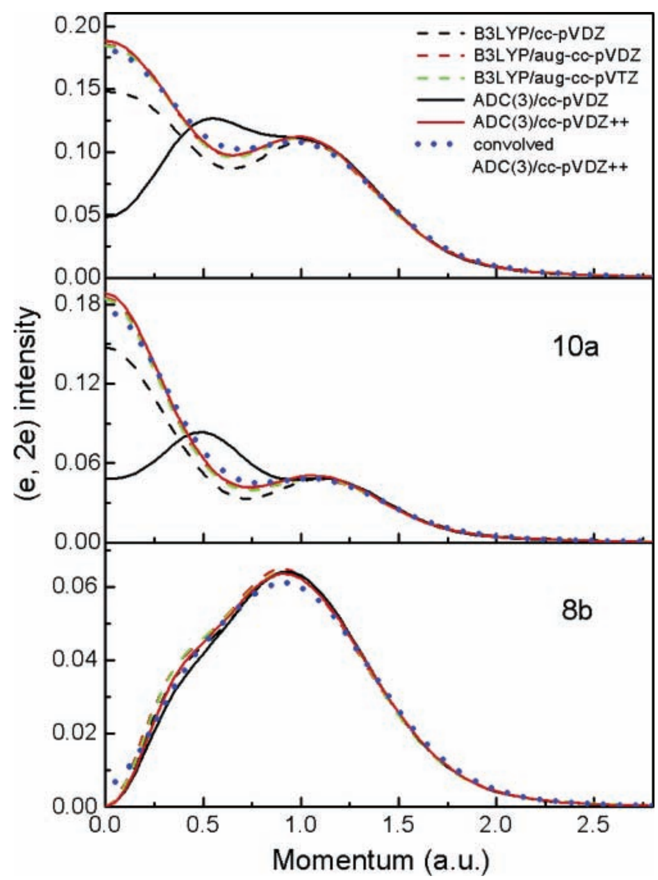

Figure 8. Dyson [ADC(3)] orbital and Kohn−Sham [B3LYP] electron momentum distributions for band III, encompassing the contributions of orbitals 10a and 8b, along with the individual orbital contributions.

Theoretical momentum profiles for the peak (III) at ∼13.3 eV that has been ascribed to the 10a and 8b orbitals are presented in Figure 8. The statement that diffuse functions play an essential role in accurate computations of orbital densities at low electron momenta is particularly true for orbital 10a (Figure 8). These computations corroborate our analysis of the intensity characterizing the $n_\sigma(sp^2)$ signal at ∼13.2 eV in the experimental (e,2e) spectrum measured at $\phi = 0°$, and confirms therefore our suggestion that momentum distributions very specifically fingerprint the outcome of through-bond and through-space orbital interactions due to the anomeric effect at these electron binding energies. Whereas the ADC(3)/cc-pVDZ results clearly failed to provide reliable insights into the available (e,2e) intensities for the 10a ionization channel, the B3LYP/cc-pVDZ and ADC(3)/cc-pVDZ++ momentum distributions are rather similar. These observations provide support to our suggestion that the overall great successes of density functional theory in modeling the results of EMS experiments may be due to a cancellation of errors due, among others, to basis set limitations, the too rapid decay of the electronic potential at

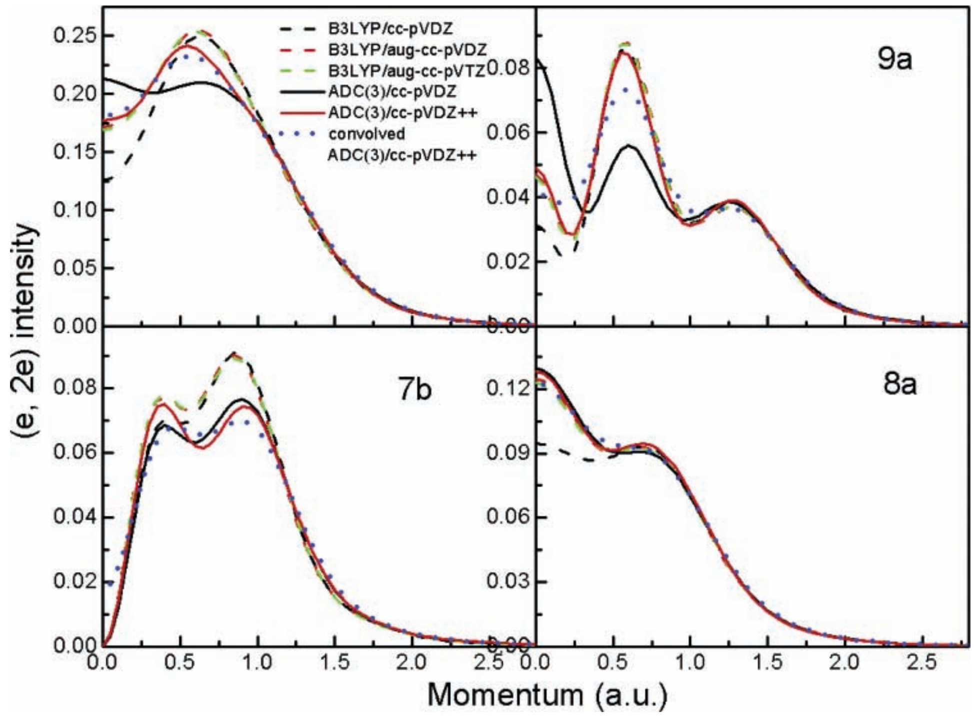

Figure 9. Dyson [ADC(3)] orbital and Kohn−Sham [B3LYP] electron momentum distributions for band IV, encompassing the contributions of orbitals 9a, 7b, and 8a, along with the individual orbital contributions.

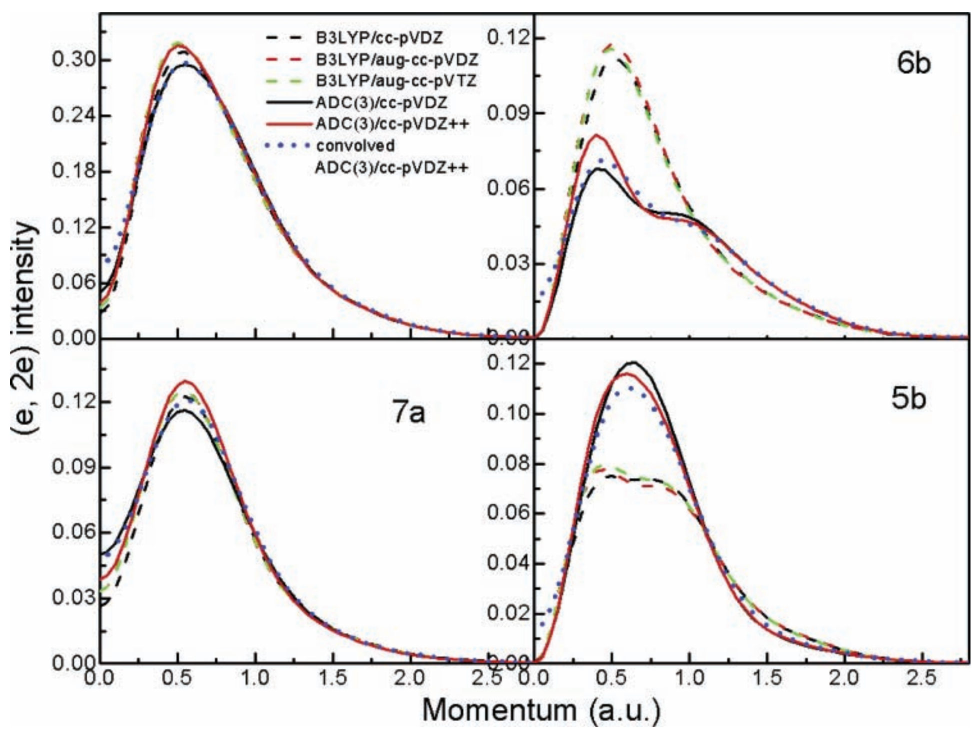

Figure 10. Dyson [ADC(3)] orbital and Kohn−Sham [B3LYP] electron momentum distributions for band V, encompassing the contributions of orbitals 6b, 7a, and 5b, along with the individual orbital contributions.

large molecular distances, and, last but not least, the neglect of electronic relaxation effects with standard functionals such as B3LYP.

The shape of the momentum distribution calculated for the band (IV) at ∼15.1 eV by summing the contributions from the 9a, 7a, and 8a orbitals (Figure 9) also strongly varies, depending on the presence or not of diffuse functions in the basis set. Without diffuse functions, very significant differences are observed between the total and individual B3LYP Kohn−Sham and ADC(3) Dyson orbital momentum distributions. Despite the intricate appearance of the individual orbital momentum distributions, these distributions almost converge to the same profile when diffuse functions are incorporated. This profile exhibits then a shallow minimum at $p \sim 0$ au, and a single maximum at $p \sim 0.53$ au. The 8a and 7b momentum distributions exhibit *two* main components. Besides the maxima that are normally expected for a s-type or p-type profile, the excess component at large p values indicates in both cases extra confinement by *one* symmetrically nonredundant nodal surface that coincides with the O−CH_3 bonds. The individual momen-

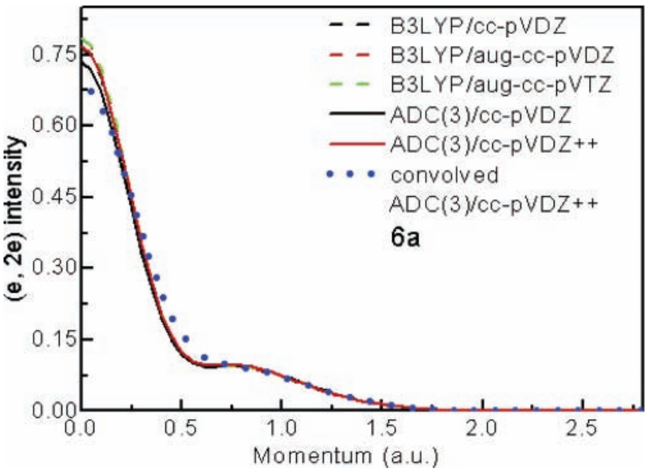

Figure 11. Dyson [ADC(3)] orbital and Kohn−Sham [B3LYP] orbital momentum distributions for orbital 6a, associated with band VI.

tum distribution for the 9a orbital consists of *three* main components at $p \sim 0.00$, $\sim$0.56, and $\sim$1.28 au, which in turn indicates also a very intricate orbital topology. By virtue of spherical averaging, the latter two maxima may here be very logically ascribed to the presence of *two* symmetrically nonredundant nodal surfaces, with the first one across the O−C(H_2) bond and the second one across the O−C(H_3) bond.

Due to the more limited number of nodal surfaces, the appearance of the individual orbital momentum distributions simplifies (Figure 10) when reaching the bottom of the outer-valence region, defined by the band (V) at $\sim$17.1 eV which finds its origin in ionization of the 6b, 7a, and 5b orbitals. The predominance of b-type orbitals at these electron binding energies explains the p-type profile for the summed momentum distributions. Also, the 7a orbital is characterized by one nodal surface that follows the C−O−C−O−C backbone, which explains why the corresponding (e,2e) spherically averaged ionization cross sections almost vanish at zero momenta, despite the symmetry of the orbital. Comparison of the momentum distributions associated with the 6b and 5b orbitals seems to indicate a reversal of the energy order for the corresponding one-electron ionization channels at the B3LYP and ADC(3) levels. More specifically, due to the noncrossing rule between orbitals or wave functions belonging to the same irreducible representation of a given symmetry point group,[82] very strong atomic orbital mixing between the two former levels is expected, with regard to an energy interval of only $\sim$0.3 eV. Compared with the outermost momentum distributions, the differences observed among the various models for the total momentum density associated with band V are very limited.

In line with the latter remark, we observe (Figure 11) an almost perfect agreement between the various predictions made for the 6a level marking the top of the inner-valence C 2s band at $\sim$20.6 eV. Besides a maximum in the related (e,2e) ionization intensity at $p \sim 0.00$ au, due to the a-type symmetry of the orbital, a broader component seen at $p \sim 0.74$ au can be related to the confinement of the electron density by a nodal surface that approximately follows the C−O−C−O−C backbone. Beyond this point, the orbital picture of ionization is no longer strictly valid, as shake-up processes come into play.

For the sake of completeness, we nonetheless provide in Figure 12 the results of our calculations for the innermost C_{2s} bands (VII, VIII) at $\sim$22.8 and $\sim$23.9 eV ascribed to shake-up lines from the 4b and 5a orbitals, and obtained by summing at the ADC(3) level the momentum distributions recovered from the *un-normalized* Dyson orbitals for each identified shake-up line at these binding energies (the employed total pole strength being then given in parentheses). Except for the loss of ionization intensity in further unidentified shake-up processes that should contribute to a correlation tail at much higher binding energies,[70] it is clear that the B3LYP Kohn−Sham orbitals and the ADC(3) Dyson orbitals lead to almost equal momentum distributions. This observation is in phase with the idea that shake-up states "borrow" their intensity to specific one-electron levels. In this energy region, diffuse functions have no influence at all on the computed electron momentum distributions, reflecting the strongly localized nature of these levels. Besides the maximum at $p \sim 0.0$ au due to the symmetry of the 5a orbital, a second maximum at $\sim$0.62 au (ADC(3)/cc-pVDZ++ result) is seen in the momentum distribution for band VIII. This feature can be explained by the delocalization of the orbital around all three carbons and by the presence of a single nodal surface that twice crosses the C−O−C−O−C backbone. In contrast, orbital 4b merely localizes around the end methyl groups, and a simple p-type profile is correspondingly computed for band VII.

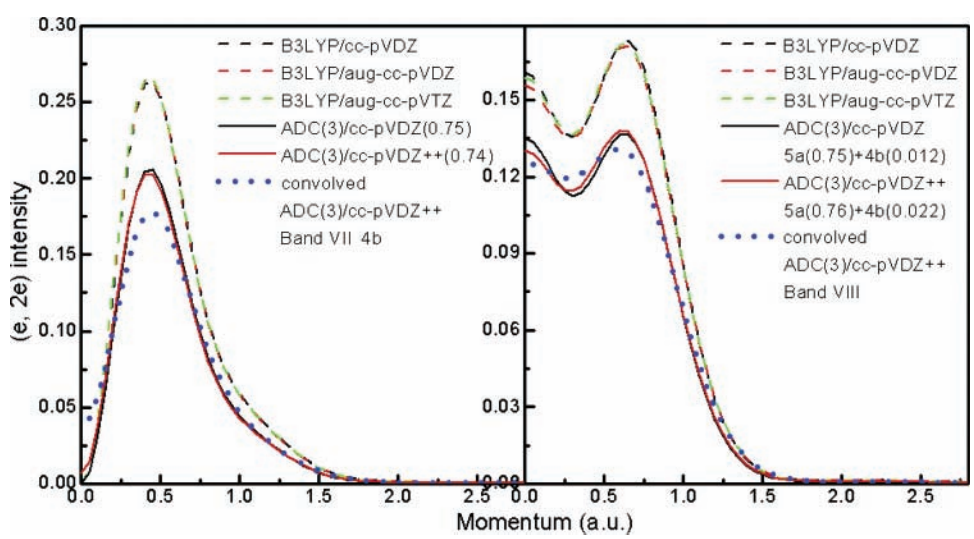

Figure 12. Un-normalized Dyson [ADC(3)] orbital and normalized Kohn−Sham [B3LYP] orbital momentum distributions for bands VII and VIII, using at the ADC(3) level the results obtained for the associated shake-up lines.

Conclusions and Outlook for the Future

A thorough theoretical study of the molecular structure, conformational equilibrium in the gas phase, ionization spectrum, and related Dyson orbital momentum distributions of dimethoxymethane has been presented, in order to establish once and for all the theoretical guidelines that should be followed for interpreting experiments on conformationally versatile molecules employing electron momentum spectroscopy. To carry out reliable enough analyses of such experiments, one should necessarily and systematically proceed through (1) a determination of relative conformer energies within an accuracy of a few tenths kilojoules per mole, on the basis of large-scale many-body quantum mechanical treatments; (2) an evaluation of the conformer abundances within a few percent accuracy, by means of statistical thermodynamics beyond the rigid rotor–harmonic oscillator (RRHO) approximation; (3) a simulation of the valence ionization spectrum, within an accuracy of a few tenths of an electronvolt, and a computation of the related transition moments for the main conformers, taking into account the dispersion of the ionization intensity over secondary shake-up states; and (4) a computation of spherically averaged electron momentum distributions for each identified ionization channel or resolvable band, taking into account the fact that the molecular conformation may have a very strong influence on the orbital energies and therefore ionization bands.[18,77]

In the present work, these goals have been achieved by using (1) the principles of a focal point analysis of energy differences computed at various [HF, MP2, MP3, CCSD, and CCSD(T)] levels and supplemented by appropriate extrapolations to the limit of an asymptotically complete basis set, (2) the protocol by Ayala and Schegel[60] for treating the internal rotation modes, (3) one-particle Green's function theory along with the ADC(3) scheme for computing one-electron and 2h-1p shake-up ionization energies along with the related transition moments, and (4) an adaptation of the MOMAP methodology by Brion et al.[74] for Fourier transforming to momentum space and spherically averaging the related Dyson orbitals, taking into account the finite angular resolution of the (e,2e) spectrometers for convolving the momentum distributions.

The main conclusions drawn from these calculations are the following. (1) According to our best estimates, the G^+G^+, TG, G^+G^-, and TT conformers of dimethoxymethane have, at 0 K and regardless of zero-point vibrational effects, relative energies equal to 0.00, 10.88, 16.08, and 23.64 kJ/mol, respectively. (2) At room temperature, these energy differences and Gibbs free energy corrections yield correspondingly molar fractions equal to 0.959, 0.026, 0.015, and 0.000. (3) A confrontation with available high-resolution photoelectron measurements corroborates the finding that only one conformer (G^+G^+) dominates at room temperature in the gas phase. Also, a comparison with available (e,2e) ionization spectra enables us to identify specific fingerprints of through-space orbital interactions associated with the anomeric effect, an observation which should motivate detailed experimental studies of electron momentum distributions throughout the outer-valence region and beyond. The one-electron picture of ionization remains indeed valid up to electron binding energies of ~22 eV. (4) At last, very significant differences have been noted in several cases between momentum distributions computed using the ADC(3) Dyson orbitals or the Kohn–Sham orbitals correspondingly derived from DFT calculations employing the B3LYP functional. These discrepancies and a significantly different dependence toward the presence of diffuse functions in the basis set reflect on the one hand well-known shortcomings of this functional in the asymptotic region (see ref 4l, 4o, and references therein) and on the other hand the fact that the low symmetry (C_2) of the molecule in its G^+G^+ conformation enables strong orbital mixing and opens up many possibilities for configuration interactions in the ground (neutral) and final (cationic) states.

Therefore, besides recommending ADC(3) for quantitatively deciphering highly congested ionization spectra, this work advocates a systematic use of ADC(3) Dyson orbitals in further analyses of EMS experiments, in order to safely identify complications such as variations of the molecular conformation,[8] distorted wave effects,[68] nuclear dynamics,[3p] or a dispersion of the ionization intensities into shake-up processes.[4,5,8,18,73]

Acknowledgment. All calculations presented in this work have been performed on Compaq ES45 and ES47 workstations at Hasselt University, Belgium. This work has been supported by the FWO-Vlaanderen, the Flemish branch of the Belgian National Science Foundation, and by the Bijzonder OnderzoeksFonds of Hasselt University. Y.R.H. worked for 9 months (June 15, 2006–March 14, 2007) as a Ph.D. student at Hasselt University, thanks to a fellowship obtained within the framework of a bilateral program for scientific cooperation between Belgium (Flanders) and the People's Republic of China. Y.R.H. and J.K.D. acknowledge financial support from the National Natural Science Foundation of China under Project No. 10575062 and by the Specialized Research Fund for the Doctoral Program of Higher Education under Project No. 20050003084. B.H. was a postdoctoral researcher at Hasselt University from July 1 to Dec 31, 2006, and acknowledges financial support from the Technical University of Budapest, Hungary, from Feb 1 to April 30, 2007.

References and Notes

(1) (a) McCarthy, I. E.; Weigold, E. *Rep. Prog. Phys.* **1991**, *54*, 789. (b) Coplan, M. A.; Moore, J. H.; Doering, J. P. *Rev. Mod. Phys.* **1994**, *66*, 985. (c) Weigold, E.; McCarthy, I. E. *Electron Momentum Spectroscopy*; Kluwer Academic/Plenum Publishers: New York, 1999. (d) McCarthy, I. E.; Weigold, E. *Rep. Prog. Phys.* **1988**, *51*, 299.

(2) (a) Braidwood, S. W.; Brunger, M. J.; Konovalov, D. A.; Weigold, E. *J. Phys. B* **1993**, *26*, 1655. (b) Rolke, J.; Cann, N.; Zheng, Y.; Hollebone, B. P.; Brion, C. E.; Wang, Y. A.; Davidson, E. R. *Chem. Phys.* **1995**, *201*, 1. (c) Duffy, P. *Can. J. Phys.* **1996**, *74*, 763. (d) Rolke, J.; Brion, C. E.; *Chem. Phys.* **1996**, *207*, 173. (e) Rolke, J.; Zheng, Y.; Brion, C. E.; Shi, Z.; Wolfe, S.; Davidson, E. R. *Chem. Phys.* **1999**, *244*, 1. (f) Zheng, Y.; Pang, W. N.; Shang, R. C.; Chen, X. J.; Brion, C. E.; Ghanty, T. K.; Davidson, E. R. *J. Chem. Phys.* **1999**, *111*, 9526.

(3) (a) Fuss, I.; McCarthy, I. E.; Minchington, A.; Weigold, E.; Larkins, F. P. *Chem. Phys.* **1981**, *63*, 19. (b) Weigold, E.; Zheng, Y.; von Niessen, W. *Chem. Phys.* **1991**, *150*, 405. (c) Rolke, J.; Brion, C. E.; Cahravorty, S. J.; Davidson, E. R.; McCarthy, I. E. *Chem. Phys.* **1997**, *215*, 191. (d) Vos, M.; Canney, S. A.; McCarthy, I. E.; Utteridge, S.; Michaelwicz, M. T.; Weigolf, E. *Phys. Rev. B* **1997**, *56*, 1309. (e) Takahashi, M.; Otsuka, K.; Udagawa, Y. *Chem. Phys.* **1998**, *227*, 375. (f) Takahashi, M.; Ogino, R.; Udagawa, Y. *Chem. Phys. Lett.* **1998**, *288*, 821. (g) Takahashi, M.; Ogino, T.; Udagawa, Y. *Chem. Phys. Lett.* **1998**, *288*, 714. (h) Adcock, W.; Brunger, M. J.; McCarthy, I. E.; Michlewicz, M. T.; von Niessen, W.; Wang, F.; Weigold, E.; Winkler, D. A. *J. Am. Chem. Soc.* **2000**, *122*, 3892. (i) Chen, X. J.; Jia, C. C.; Xu, C. K.; Ouyang, G.; Peng, L. L.; Tian, S. X.; Xu, K. Z. *Chem. Phys. Lett.* **2000**, *319*, 76. (j) Litvinyuk, I. V.; Zheng, Y.; Brion, C. E. *Chem. Phys.* **2000**, *253*, 41. (k) Litvinyuk, I. V.; Zheng, Y.; Brion, C. E.; *Chem. Phys.* **2000**, *261*, 289. (l) Deng, J. K.; Li, G. Q.; He, Y.; Huang, J. D.; Deng, H.; Wang, X. D.; Wang, F.; Zhang, Y. A.; Ning, C. G.; Gao, N. F.; Wang, Y.; Chen, X. J.; Zheng, Y. J. *Chem. Phys.* **2001**, *114*, 882. (m) Litvinyuk, I. V.; Young, J. B.; Zheng, Y.; Cooper, G.; Brion, C. E. *Chem. Phys.* **2001**, *263*, 195. (n) Tixier, S.; Shapley, W. A.; Zheng, Y.; Chong, D. P.; Brion, C. E.; Shi, Z.; Wolfe, S. *Chem. Phys.* **2001**, *270*, 263. (o) Knippenberg, S.; Nixon, K. L.; Brunger, M. J.; Maddern, T.; Campbell, L.; Trout, N.; Wang, F.; Newell, W. R.; Deleuze, M. S.; François, J.-P.; Winkler, D. A. *J. Chem. Phys.* **2004**, *121*, 10525. (p) Knippenberg, S.; Deleuze, M. S.; Cleij, T. J.; François, J.-P.; Cederbaum, L. S.; Eland, J. H. D. *J. Phys. Chem. A* **2005**, *109*, 4267.

(4) (a) Cederbaum, L. S. *J. Phys. B* **1975**, *8*, 290. (b) Cederbaum, L. S. *J. Chem. Phys.* **1975**, *62*, 2160. (c) Cederbaum, L. S.; Domcke, W.; Schirmer, J.; von Niessen, W.; Diercksen, G. H. F.; Kraemer, W. P. *J. Chem. Phys.* **1978**, *69*, 1591. (d) Cederbaum, L. S.; Domcke, W.; Schirmer, J.; von Niessen, W. *Adv. Chem. Phys.* **1986**, *65*, 115. (e) Deleuze, M. S.; Cederbaum, L. S. *Int. J. Quantum Chem.* **1997**, *63*, 465. (f) Deleuze, M. S.; Giuffreda, M. G.; François, J.-P.; Cederbaum, L. S. *J. Chem. Phys.* **1999**, *111*, 5851. (g) Deleuze, M. S.; Cederbaum, L. S. *Adv. Quantum Chem.* **1999**, *35*, 77. (h) Deleuze, M. S.; Giuffreda, M. G.; François, J.-P.; Cederbaum, L. S. *J. Chem. Phys.* **2000**, *112*, 5325. (i) Deleuze, M. S.; Giuffreda, M. G.; François, J.-P. *J. Phys. Chem. A* **2002**, *106*, 5626. (j) Deleuze, M. S.; Trofimov, A. B.; Cederbaum, L. S. *J. Chem. Phys.* **2001**, *115*, 5859. (k) Deleuze, M. S. *J. Chem. Phys.* **2002**, *116*, 7012. (l) Deleuze, M. S. *J. Phys. Chem. A* **2004**, *108*, 9244. (m) Potts, A. W.; Holland, D. M. P.; Trofimov, A. B.; Schirmer, J.; Karlsson, L.; Siegbahn, K. *J. Phys. B: At., Mol. Opt. Phys.* **2003**, *36*, 3129. (n) Kishimoto, N.; Hagihara, Y.; Ohno, K.; Knippenberg, S.; François, J.-P.; Deleuze, M. S. *J. Phys. Chem. A* **2005**, *109*, 10535. (o) Deleuze, M. S. *Chem. Phys.* **2006**, *329*, 22. (p) Potts, A. W.; Edvardson, D.; Karlsson, L.; Holland, D. M. P.; MacDonald, M. A.; Hayes, M. A.; Maripuu, R.; Siegbahn, K.; von Niessen, W. *Chem. Phys.* **2000**, *254*, 385. (q) Trofimov, A. B.; Schirmer, J.; Holland, D. M. P.; Karlsson, L.; Maripuu, R.; Siegbahn, K.; Potts, A. W. *Chem. Phys.* **2001**, *263*, 167. (r) Potts, A. W.; Trofimov, A. B.; Schirmer, J.; Holland, D. M. P.; Karlsson, L. *Chem. Phys.* **2001**, *271*, 337. (s) Trofimov, A. B.; Schirmer, J.; Holland, D. M. P.; Potts, A. W.; Karlsson, L.; Maripuu, R.; Siegbahn, K. *J. Phys. B* **2002**, *35*, 5051.

(5) Knippenberg, S.; François, J.-P.; Deleuze, M. S. *J. Comput. Chem.* **2006**, *27*, 1703.

(6) Neville, J. J.; Zheng, Y.; Hollebone, B. P.; Cann, N. M.; Brion, C. E.; Kim, C.-K.; Wolfe, S. *Can. J. Phys.* **1996**, *74*, 773.

(7) Neville, J. J.; Zheng, Y.; Brion, C. E. *J. Am. Chem. Soc.* **1996**, *118*, 10553.

(8) Deleuze, M. S.; Pang, W. N.; Salam, A.; Shang, R. C. *J. Am. Chem. Soc.* **2001**, *123*, 4049.

(9) Pang, W. N.; Gao, J. F.; Ruan, C. J.; Shang, R. C.; Trofimov, A. B.; Deleuze, M. S. *J. Chem. Phys.* **2000**, *112*, 8043.

(10) Pang, W. N.; Shang, R. C.; Gao, J. F.; Gao, N. F.; Chen, X. J.; Deleuze, M. S. *Chem. Phys. Lett.* **1998**, *296*, 605.

(11) McQuarrie, D. A. *Statistical Mechanics*; Harper and Row: New York, 1976.

(12) Linderberg, J.; Öhrn, Y. *Propagators in Quantum Chemistry*; Wiley: Hoboken, NJ, 2004.

(13) Cederbaum, L. S.; Domcke, W. *Adv. Chem. Phys.* **1977**, *36*, 205.

(14) Öhrn, Y.; Born, G. *Adv. Quantum Chem.* **1981**, *13*, 1.

(15) von Niessen, W.; Schirmer, J.; Cederbaum, L. S. *Comput. Phys. Rep.* **1984**, *1*, 57.

(16) Ortiz, J. V. *Computational Chemistry: Reviews of Current Trends*; Leszczynski, J., Ed.; World Scientific: Singapore, 1997; Vol. 2, p 1.

(17) (a) Schirmer, J.; Cederbaum, L. S.; Walter, O. *Phys. Rev. A* **1983**, *28*, 1237. (b) Schirmer, J.; Angonoa, G. *J. Chem. Phys.* **1989**, *91*, 1754. (c) Weikert, H.-G.; Meyer, H.-D.; Cederbaum, L. S.; Tarantelli, F. *J. Chem. Phys.* **1996**, *104*, 7122.

(18) Deleuze, M. S.; Knippenberg, S. *J. Chem. Phys.* **2006**, *125*, 104309.

(19) Saha, S.; Wang, F.; Falzon, C. T.; Brunger, M. J. *J. Chem. Phys.* **2005**, *123*, 124315.

(20) Brunger, M. J.; Winkler, D. A.; Michalewicz, M. T.; Weigold, E. *J. Chem. Phys.* **1998**, *108*, 1859.

(21) (a) Burkert, U.; Allinger, N. L. *Molecular Mechanics*; ACS Monograph: Washington, DC, 1982; Vol. 177. (b) Eliel, E. L.; Allinger, N. L.; Angyal, S. J. *Conformational Analysis*; Interscience Publishers: New York, 1967.

(22) Kneisler, J. R.; Allinger, N. L. *J. Comput. Chem.* **1996**, *17*, 757.

(23) Venkatesan, V.; Sundararajan, K.; Sankaran, K.; Viswanathan, K. S. *Spectrochim. Acta, Part A* **2002**, *58*, 467.

(24) Wiberg, K. B.; Murcko, M. A. *J. Am. Chem. Soc.* **1989**, *111*, 4821.

(25) Deslongchamps, P. *Stereoelectronic Effects in Organic Chemistry*; Pergamon Press: Oxford, 1983.

(26) Kirby, A. J.: *The Anomeric Effects and Related Stereoelectronic Effects at Oxygen*; Springer-Verlag: Berlin, 1983.

(27) Werstiuk, N. H.; Laidig, K. E.; Ma, J. Application of Quantum Theory of Atoms in Molecules to Study of Anomeric Effect in Dimethoxymethane. *ACS Symp. Ser.* **1993**, *539*, 176.

(28) Trapp, M. L.; Watts, J. K.; Weinberg, N.; Pinto, B. M. *Can. J. Chem.* **2006**, *84*, 692.

(29) Smith, G. D.; Jaffe, R. L.; Yoon, D. Y. *J. Phys. Chem.* **1994**, *98*, 9072.

(30) Lemieux, R. U. In *Molecular rearrangements*; de Mayo, P., Ed.; Wiley: New York, 1964; Vol. 2, p 709.

(31) Edward, J. T. *Chem. Ind. (London)* **1955**, 1102.

(32) Aoki, K. *J. Chem. Soc. Jpn.* **1953**, *74*, 110.

(33) (a) Astrup, E. E. *Acta Chem. Scand.* **1971**, *25*, 1494. (b) Astrup, E. E.; *Acta Chem. Scand.* **1973**, *27*, 3271.

(34) Abe, A.; Inomata, K.; Tanisawa, E.; Ando, I. *J. Mol. Struct.* **1990**, *238*, 315.

(35) Yokoyama, Y.; Ohashi, Y. *Bull. Chem. Soc. Jpn.* **1999**, *72*, 2183.

(36) (a) Favero, L. B.; Caminati, W.; Velino, B. *Phys. Chem. Chem. Phys.* **2003**, *5*, 4776. (b) Kavitha, V.; Sundararajan, K.; Viswanathan, K. S. *J. Phys. Chem. A* **2005**, *109*, 9259.

(37) Schwarz, W. H. E. *Angew. Chem.* **2006**, *45*, 1508.

(38) Jørgensen, F. S. *J. Chem. Res., Synop.* **1981**, 212.

(39) Jeffrey, G. A.; Pople, J. A.; Binkley, J. S.; Vishveshwara, S. *J. Am. Chem. Soc.* **1978**, *100*, 373.

(40) Tvaroska, I.; Bleha, T. *J. Mol. Struct.* **1975**, *24*, 249.

(41) Wolfe, S.; Whangbo, M.-H.; Mitchell, D. *J. Carbohydr. Res.* **1979**, *69*, 1.

(42) (a) Schäfer, L.; Van Alsenoy, C.; Williams, J. O.; Scarsdale, J. N.; Geise, H. J. *THEOCHEM* **1981**, *76*, 349. (b) Williams, J. O.; Van Alsenoy, C.; Schäfer, L. *THEOCHEM* **1981**, *76*, 109.

(43) (a) Lee, C.; Yang, W.; Parr, R. G. *Phys. Rev. B* **1998**, *37*, 785. (b) Becke, A. D. *J. Chem. Phys.* **1993**, *98*, 5648.

(44) Allinger, N. L.; Fermann, J. T.; Allen, W. D.; Schaefer, H. F., III. *J. Chem. Phys.* **1997**, *106*, 5143.

(45) Salam, A.; Deleuze, M. S. *J. Chem. Phys.* **2002**, *116*, 1296.

(46) Kwasniewski, S. P.; Claes, L.; François, J.-P.; Deleuze, M. S. *J. Chem. Phys.* **2003**, *118*, 7823.

(47) Deleuze, M. S.; Claes, L.; Kryachko, E. S.; François, J.-P. *J. Chem. Phys.* **2003**, *106*, 8569.

(48) Szabo, A.; Ostlund, N. S. *Modern Quantum Chemistry*; McGraw-Hill: New York, 1982.

(49) Scuseria, G. E.; Lee, T. J. *J. Chem. Phys.* **1990**, *93*, 5851.

(50) (a) Purvis, G. D.; Bartlett, R. J. *J. Chem. Phys.* **1982**, *76*, 1910. (b) Scuseria, G. E.; Janssen, C. L.; Schaefer, H. F., III. *J. Chem. Phys.* **1988**, *89*, 7382. (c) Raghavachari, K.; Trucks, G. W.; Head-Gordon, M.; Pople, J. A. *Chem. Phys. Lett.* **1989**, *157*, 479. (d) Bartlett, R. J. *J. Phys. Chem.* **1989**, *93*, 1697.

(51) (a) Pitzer, K. S.; Gwinn, W. D. *J. Chem. Phys.* **1942**, *10*, 428. (b) Li, C. M.; Pitzer, K. S. *J. Phys. Chem.* **1956**, *60*, 466. (c) Truhlar, D. G. *J. Comput. Chem.* **1991**, *12*, 266. (d) Chung-Philipps, A. *J. Comput. Chem.* **1992**, *13*, 874. (e) Hu, W. P.; Truhlar, D. G. *J. Am. Chem. Soc.* **1994**, *116*, 7797. (f) Corchado, J. C.; Espinogarcia, J.; Hu, W. P.; Truhlar, D. G. *J. Phys. Chem.* **1995**, *99*, 687. (g) Heuts, J. P. A.; Gilbert, R. G.; Radom, L. *J. Phys. Chem.* **1996**, *100*, 18997. (h) Hu, W. P.; Truhlar, D. G. *J. Am. Chem. Soc.* **1996**, *118*, 860. (i) McClurg, R. B.; Flagan, R. C.; Goddard, W. A. *J. Chem. Phys.* **1997**, *106*, 6675.

(52) (a) Pickup, B. T. *Chem. Phys.* **1977**, *19*, 193. (b) McWeeny, R.; Pickup, B. T. *Rep. Prog. Phys.* **1980**, *43*, 1065. (c) Öhrn, Y.; Born, G. *Adv. Quantum Chem.* **1981**, *13*, 1. (d) Deleuze, M.; Pickup, B. T.; Delhalle, *J. Mol. Phys.* **1994**, *83*, 655. (e) Seabra, G. M.; Kaplan, I. G.; Zakrzewski, V. G.; Ortiz, J. V. *J. Chem. Phys.* **2004**, *121*, 4142. (f) Ning, C. G.; Ren, X. G.; Deng, J. K.; Su, G. L.; Zhang, S. F.; Knippenberg, S.; Deleuze, M. S. *Chem. Phys. Lett.* **2006**, *421*, 52.

(53) (a) Dunning, T. H., Jr. *J. Chem. Phys.* **1989**, *90*, 1007. (b) Kendall, R. A.; Dunning, T. H.; Harrisson, R. J. *J. Chem. Phys.* **1992**, *96*, 6796.

(54) (a) Feller, D. *J. Chem. Phys.* **1992**, *96*, 6104. (b) Feller, D. *J. Chem. Phys.* **1993**, *98*, 7059.

(55) Martin, J. M. L.; Ab Initio Thermochemistry Beyond Chemical Accuracy for First- and Second-Row Compounds. In *Energetics of Stable Molecules and Reactive Intermediates*; Mirrasda Piedade, M. E., Irikura, K. K, Eds.; NATO ASI Symposium Series; Kluwer: Dordrecht, The Netherlands, 1999.

(56) Schwartz, C. Estimating Convergence Rates of Variational Calculations. In *Methods in Computational Physics*; Alder, B. J., Ed.; Academic Press: New York, 1963; Vol. 2.

(57) (a) Van Orden, A.; Saykally, R. T. *Chem. Rev.* **1998**, *98*, 2313. (b) Martin, J. M. L.; Taylor, P. R. *J. Phys. Chem.* **1996**, *100*, 6047.

(58) (a) Martin, J. M. L.; Parthiban, S. In *Quantum Mechanical Prediction of Thermochemical Data*; Cioslowski, J., Szareka, A., Eds.; Understanding Chemical Reactivity Series 22; Kluwer: Dordrecht, The Netherlands, 2001; Chapter 2, pp 31−65. (b) Parthiban, S.; Martin, J. M. L. *J. Chem. Phys.* **2001**, *115*, 2051.

(59) (a) Martin, J. M. L.; François, J.-P.; Gijbels, R.; Almlöf, J. *Chem. Phys. Lett.* **1991**, *187*, 367. (b) Martin, J. M. L.; El Yazal, J.; François, J.-P. *Mol. Phys.* **1995**, *86*, 1437. (c) Martin, J. M. L.; El Yazal, J.; François, J.-P. *Chem. Phys. Lett.* **1995**, *242*, 570. (d) Martin, J. M. L.; El Yazal, J.; François, J.-P. *Chem. Phys. Lett.* **1996**, *252*, 9. (e) Giuffreda, M. G.; Deleuze, M. S.; François, J.-P. *J. Phys. Chem. A* **1999**, *103*, 5137. (f) Martin, J. M. L. *Spectrochim. Acta* **1999**, *55*, 11126.

(60) Ayala, P. Y.; Schlegel, H. B. *J. Chem. Phys.* **1998**, *108*, 2314.

(61) Mayo, S. L.; Olafson, B. D.; Goddard, W. A. *J. Phys. Chem.* **1990**, *94*, 8897.

(62) Frisch, M. J.; Trucks, G. W.; Schlegel, H. B.; Scuseria, G. E.; Robb, M. A.; Cheeseman, J. R.; Montgomery, J. A., Jr.; Vreven, T.; Kudin, K. N.; Burant, J. C.; Millam, J. M.; Iyengar, S. S.; Tomasi, J.; Barone, V.; Mennucci, B.; Cossi, M.; Scalmani, G.; Rega, N.; Petersson, G. A.; Nakatsuji, H.; Hada, M.; Ehara, M.; Toyota, K.; Fukuda, R.; Hasegawa, J.;

Ishida, M.; Nakajima, T.; Honda, Y.; Kitao, O.; Nakai, H.; Klene, M.; Li, X.; Knox, J. E.; Hratchian, H. P.; Cross, J. B.; Bakken, V.; Adamo, C.; Jaramillo, J.; Gomperts, R.; Stratmann, R. E.; Yazyev, O.; Austin, A. J.; Cammi, R.; Pomelli, C.; Ochterski, J. W.; Ayala, P. Y.; Morokuma, K.; Voth, G. A.; Salvador, P.; Dannenberg, J. J.; Zakrzewski, V. G.; Dapprich, S.; Daniels, A. D.; Strain, M. C.; Farkas, O.; Malick, D. K.; Rabuck, A. D.; Raghavachari, K.; Foresman, J. B.; Ortiz, J. V.; Cui, Q.; Baboul, A. G.; Clifford, S.; Cioslowski, J.; Stefanov, B. B.; Liu, G.; Liashenko, A.; Piskorz, P.; Komaromi, I.; Martin, R. L.; Fox, D. J.; Keith, T.; Al-Laham, M. A.; Peng, C. Y.; Nanayakkara, A.; Challacombe, M.; Gill, P. M. W.; Johnson, B.; Chen, W.; Wong, M. W.; Gonzalez, C.; Pople, J. A. *Gaussian 03*, revision D.01; Gaussian, Inc.: Wallingford, CT, 2004.

(63) (a) MOLPRO is a package of ab initio programs written by H.-J. Werner and P. J. Knowles, with contributions from Amos, R. D.; Bernhardsson, A.; Berning, A.; Celani, P.; Cooper, D. L.; Deegan, M. J. O.; Dobbyn, A. J.; Eckert, F.; Hampel, C.; Hetzer, G.; Korona, T.; Lindh, R.; Lloyd, A. W.; McNicholas, S. J.; Manby, F. R.; Meyer, W.; Mura, M. E.; Nicklass, A.; Palmieri, P.; Pitzer, R.; Rauhut, G.; Schütz, M.; Stoll, H.; Stone, A. J.; Tarroni, R.; and Thorsteinsson, T. (b) Hampel, C.; Peterson, K.; Werner, H.-J. *Chem. Phys. Lett.* **1992**, *190*, 1 and references therein. The program to compute the perturbative triples corrections has been developed by M. J. O. Deegan and P. J. Knowles (1992).

(64) Deleuze, M. S. *Int. J. Quantum Chem.* **2003**, *93*, 191.

(65) Schmidt, M. W.; Baldridge, K. K.; Jensen, J. H.; Koseki, S.; Gordon, M. S.; Nguyen, K. A.; Windus, T. L.; Elbert, S. T. *QCPE Bull.* **1990**, *10*, 52.

(66) (a) Ruhe, A. *Math. Comput.* **1979**, *33*, 680. (b) Meyer, H.-D.; Pal, S. *J. Chem. Phys.* **1989**, *91*, 6195.

(67) (a) Liu, B. *Numerical Algorithms in Chemistry, Algebraic Methods*; Lawrence Berkeley Laboratory: Berkeley, California; Report No. LBL-8158 (unpublished). (b) Tarantelli, F.; Sgamellotti, A.; Cederbaum, L. S.; Schirmer, J. *J. Chem. Phys.* **1987**, *86*, 2201.

(68) (a) Takahashi, M.; Saito, T.; Hiraka, J.; Udawaga, Y. *J. Phys. B: At., Mol. Opt. Phys.* **2003**, *36*, 2539. (b) Takahashi, M.; Udawaga, Y. *J. Electron Spectrosc. Relat. Phenom.* **2004**, *137*, 387.

(69) (a) Ren, X. G.; Ning, C. G.; Deng, J. K.; Zhang, S.; Sum, G.; Huang, F.; Li, G. *Chem. Phys. Lett.* **2005**, *404*, 279. (b) Su, G. L.; Ren, X, G.; Su, G. L.; Ning, C. G. *J. Chem. Phys.* **2005**, *122*, 054301. (c) Zhang, S. F.; Ren, X. G.; Su, G. L.; Ning, C. G.; Zhou, H.; Li, B.; Li, G. Q.; Deng, J. K. *Chem. Phys.* **2006**, *327*, 269.

(70) Golod, A.; Deleuze, M. S.; Cederbaum, L. S. *J. Chem. Phys.* **1999**, *110*, 6014.

(71) (a) Casida, M. E.; Jamorski, C.; Casida, K. C.; Salahub, D. R. *J. Chem. Phys.* **1998**, *108*, 4439. (b) Tozer, D. J.; Handy, N. C. *J. Chem. Phys.* **1998**, *109*, 10180. (c) Reimers, J.; Cai, Z.-L.; Bilić, A.; Hush, N. S. *Ann. N.Y. Acad. Sci.* **2003**, *110*, 235.

(72) Zhang, G.; Musgrave, C. B. *J. Phys. Chem. A* **2007**, *111*, 1554.

(73) Knippenberg, S.; Nixon, K. L.; Mackenzie-Ross, H.; Brunger, M. J.; Wang, F.; Deleuze, M. S.; François, J.-P.; Winkler, D. A. *J. Phys. Chem. A* **2005**, *109*, 9324.

(74) See various contributions to the original HEMS program as recorded by Bawagan (Bawagan, A. O. Ph.D. Thesis, University of British Columbia (UBC), 1987). The HEMS (now known as MOMAP) program has been extensively revised and extended at UBC by N. M. Cann and G. Cooper.

(75) Duffy, P.; Casida, M. E.; Brion, C. E.; Chong, D. P. *Chem. Phys.* **1992**, *159*, 347.

(76) Zheng, Y.; Neville, J. J.; Brion, C. E.; Wang, Y.; Davidson, E. R. *Chem. Phys.* **1994**, *188*, 109.

(77) (a) Deleuze, M. S.; Denis, J. P.; Pickup. B. T. *J. Phys. Chem.* **1993**, *97*, 5115. (b) Deleuze, M. S.; Delhalle, J.; Pickup, B. T.; Svensson, S. *J. Am. Chem. Soc.* **1994**, *116*, 10715. (c) Deleuze, M.; Delhalle, J.; Pickup, B. T. *J. Phys. Chem.* **1994**, *98*, 2382. (d) Deleuze, M.; Delhalle, J.; Mosely, D. H.; André, J.-M. *Phys. Scr.* **1995**, *51*, 111.

(78) Janak, J. F.; *Phys. Rev. B* **1978**, *18*, 7165.

(79) (a) Gritsenko, O. V.; Baerends, E. J. *J. Chem. Phys.* **2002**, *117*, 9154. (b) Gritsenko, O. V.; Braïda, B.; Baerends, E. J. *J. Chem. Phys.* **2003**, *110*, 1937.

(80) Boulanger, P.; Riga, J.; Verbist, J. J.; Delhalle, J. *Macromolecules* **1989**, *22*, 173.

(81) Pickup, B. T.; Goscinski, O. *Mol. Phys.* **1973**, *26*, 1013.

(82) See Lowe, J. P. *Quantum Chemistry*; Academic Press: San Diego, 1978; or any textbook of quantum chemistry.